Data assimilation of generic boundary-layer flows for wind-turbine applications - An LES study

Linus Wrba[1], Antonia Englberger[1], Andreas Dörnbrack[1], Gerard Kilroy[1], and Norman Wildmann[1]

[1]Deutsches Zentrum für Luft- und Raumfahrt, Institut für Physik der Atmosphäre, Oberpfaffenhofen, Germany

Correspondence: Linus Wrba (linus.wrba@dlr.de)

Abstract. Providing date- and site-specific turbulent inflow fields for large-eddy simulations (LES) of the flow through wind turbines becomes increasingly important for reliable estimates of power production. In this study, data assimilation techniques are applied to adapt the atmospheric inflow field towards previously defined wind profiles. A standard and a modified version of the Newtonian relaxation technique and an assimilation method based on the vibration equation are implemented in the geophysical flow solver EULAG. The extent to which they are able to adapt mean horizontal wind velocities towards target profiles and the impact on atmospheric turbulence of an idealized LES are investigated. The sensitivity of the methods to grid refinement is ~~analysed~~analyzed. The method based on the vibration equation is suited for fine grids ($dx = dy = dz = 5$ m), which ~~are necessary in~~ is a common grid resolution for wind-energy ~~applications~~studies. Furthermore, the vibration method is used to nudge the zonal and meridional inflow velocities of an idealized atmospheric simulation towards velocity profiles representing a weakly-stably-stratified atmospheric boundary layer (ABL) at the wind-farm site WiValdi at Krummendeich, Germany. On site wind measurements and the output of mesoscale simulations are evaluated to define the target velocity profile. The assimilation method based on the vibration equation is able to adapt the zonal and meridional velocity components of an atmospheric flow while ~~damping~~ negative effects on the atmospheric turbulence could be reduced. In a final step, the assimilated flow field is taken as inflow for a wind-turbine simulation, which then shows the characteristic structures of a wake in the ABL. This study shows the suitability of the vibration ~~assimilation technique~~ method for adapting inflow fields for wind energy purposes and presents the advantages and disadvantages of the method.

Keywords: LES, data assimilation, atmospheric boundary layer, wind-turbine wake

1 Introduction

The growing demand for wind energy is accompanied with a wide range of challenges as structural components and technical characteristics of wind turbines are getting more and more sophisticated. In particular, the mutual interaction of wind-turbine wakes in wind farms and their response to the transient atmospheric flow field are grand challenges in wind-energy research (cf.

Veers et al., 2023). General attention is paid to the performance of the turbines and the loads on the blades which are mainly ~~controlled~~ determined by turbulence in the ABL (cf. Hansen, 2013; Wharton and Lundquist, 2012). The general question is how to maximize the harvested power of a wind turbine at a certain location under specific operational conditions. One of the decisive factors in answering this question is the atmospheric situation under which the wind turbines are operating. Knowledge of the thermal stratification and the flow conditions is becoming increasingly important because rotor diameters are getting larger and the hub heights are getting higher, thus covering a greater depth of the ABL. A better knowledge of the impact of different atmospheric characteristics like the vertical gradient of the horizontal velocity and turbulence intensities impacting a wind turbine and its wake is therefore essential~~, especially for wind parks with multiple turbines~~.

The recent opening of the ~~research wind park~~ wind energy research farm WiValdi[1] (Wind Validation) in Krummendeich, North Germany on 15 August 2023 by the German Aerospace Center (DLR) and the Research Alliance Wind Energy (FVWE[2]) offers a timely opportunity to expand our knowledge on this topic. The wind park consists of two Enercon E-115 EP3 turbines with hub heights of 92 m and rotor diameters of $D = 116$ m separated by a rather narrow spacing of 4.4 D. In addition, a smaller custom-built turbine is currently under construction. The flow fields and the turbine wakes at the wind park can be measured in great detail by the vast observational network located on site. This network includes a series of measuring masts, multiple Doppler wind lidar (DWL) instruments, and a microwave radiometer.

Even with a really dense observational network and a large number of field measurements that can provide quasi-reliable 3-D pictures of the atmospheric situation, there are still natural spatial and temporal limitations in resolving all motion modes affecting the response of wind turbines to the atmospheric flow. In order to close such scale gaps, numerical simulations can provide 3-D flow fields of the entire wind park with very high spatial and temporal resolutions. In particular, LES models have been proven to be a useful and powerful tool to compute these turbulent flow fields. In contrast to simulations based on Reynolds-averaged Navier-Stokes (RANS) equations, LESs are capable of resolving turbulence in the flow. In addition, LESs are computationally less expensive than direct numerical simulations (DNS) because the subgrid-scale (SGS) contribution to the turbulence is parameterized.

LESs are also frequently used to evaluate the effects of thermal stratification of the ABL on the wakes of wind turbines and wind farms for various atmospheric conditions (cf. Bhaganagar and Debnath, 2014; Abkar et al., 2016; Vollmer et al., 2016; Englberger and Dörnbrack, 2018). Particular emphasis has been placed on a distinctive thermal ABL stratification (neutral, convective, stable) on the flow around a single wind turbine and the flow in a wind farm (Porté-Agel et al., 2020). However, the majority of these studies conduct their basic research with idealized LESs, that are characterized by no large- and mesoscale forcing and by no temporal or spatial variation of the associated pressure gradient. The representation of real, measured flow conditions like those observed in WiValdi, however, cannot be addressed reliably with such purely idealized setups.

One way to generate site-specific atmospheric flow conditions is to couple mesoscale simulations (e.g. simulations of the Weather Research and Forecasting Model (WRF) (Skamarock et al., 2019)) with LESs (e.g., Aitken et al., 2014; Sanchez Gomez and Lundquist, 2020; Kilroy et al., 2024). Recent advances in this research field has been made by the Mesoscale to Microscale

[1] https://windenergy-researchfarm.com

[2] Forschungsverbund Windenergie https://www.fvwe.uni-oldenburg.de

Coupling project sponsored by the U.S. Department of Energy (cf., Haupt et al., 2022). There, the authors emphasize the complexity of modeling the correct energy transfer from the largest scales of motion to the scales within the ABL from which the wind turbines generate electrical energy. Further, they note that simulations from the mesoscale down to the microscale (for example, with the mentioned WRF-LES coupling) are ~~computationally exceptionally~~ exceptionally computationally expensive. Therefore, such elaborate methods cannot be used to simulate a variety of different atmospheric situations, assuming that both the computing time and the physical time required to perform the simulations are far too long. Other approaches including a technique that combines atmospheric modeling and machine learning try to generate time-resolved wind inflow data for turbines (cf. Rybchuk et al. (2025)).

An alternative approach to circumvent the expensive meso- and microscale coupling is to conduct idealized numerical simulations coupled with a suitable data-assimilation method for providing date- and site specific turbulent flow conditions. This numerical approach is computationally less expensive. In such a setup, ~~the~~ data-assimilation ~~method is~~ methods are assumed to transfer the given mesoscale information (wind and stability profiles) onto the microscale (cf., Stauffer and Seaman, 1990; Neggers et al., 2012; Maronga et al., 2015; Nakayama and Takemi, 2020; Allaerts et al., 2020).

In general, those methods apply a damped harmonic oscillator as an additional forcing in the governing equations of motion. Commonly, this forcing term can consist of a damping (proportional) and an oscillating (integral) part ~~(e.g., ?)~~ (e.g., Spille-Kohoff and Kaltenbach, 2001). In the case of Newtonian relaxation, only the damping part is considered. Here, the numerically calculated profiles of wind, temperature, humidity etc. are adjusted to given target profiles (which can either come from measurements or are extracted from the output of mesoscale model simulations) using a specific relaxation time scale, which is a free parameter of this method.

The relaxation time scale should be long enough ($\sim$ hours) that the small-scale turbulence in the LES is not affected by it, however, it needs to be small enough to be able to adapt the LES towards mesoscale characteristics in a reasonable time (Neggers et al., 2012). An issue, however, is that turbulence intensity is often overly reduced using Newtonian relaxation. ~~To circumvent this limitation, the damping term has been modified in~~ The investigations by Allaerts et al. (2020) and Allaerts et al. (2023) ~~. Their~~ present an 'indirect profile assimilation' method~~uses~~. It is described as an internal forcing technique deduced from mesoscale variables (wind speed and temperature), including the time and height history of these variable in the LES. Their grid assimilation method acts in the numerical simulation at every grid point in the domain and achieves an equilibrium state with the desired atmospheric mean characteristics and turbulent statistics. They tested the approach with the damping part, and a combination of both damping and oscillating, with quite similar results. Further, Stipa et al. (2024) developed another domain relaxation approach by applying the proportional and integral part, which is additionally able to prevent inertial oscillations, making it well suited for wind-park approaches.

Another data-assimilation technique described in Nakayama and Takemi (2020) is based on the oscillating part only, which has the property of fluctuating around the target mean values. This integral forcing is controlled by the natural frequency of the flow field, which has to be set appropriately in order not to damp turbulent fluctuations. We refer to this method in the following as the vibration method. ~~Nakayama and Takemi (2020) emphasised~~ Their approach includes a precursor simulation driven by a pressure gradient. This precursor is used as inflow for a following simulation where the assimilation technique is applied only in a nudging area which is smaller than the simulation domain. Nakayama and Takemi (2020) emphasized the advantage of this method in handling the turbulence intensity in comparison to the Newtonian damping.

While the ~~method of Allaerts et al. (2020) has~~ methods of Allaerts et al. (2020) and Stipa et al. (2024) have been directly developed for wind-turbine applications, the method of Nakayama and Takemi (2020) has been applied only at a rather coarse resolution of 40 m horizontally and relaxes only the horizontal wind field. However, the application of this method to ~~high-resolution~~ higher resolved LESs including wind turbines would have the advantage that it can reproduce an assimilation of simultaneous measurements, is not limited to horizontal homogeneity and ~~can~~ could possibly be applied in complex terrain. Therefore, it also seems well-suited for wind-energy applications. Considering the DLR wind-farm WiValdi, it seems to be a worthwhile endeavor to modify the method of Nakayama and Takemi (2020) so that it can be applied ~~to~~ in this first approach to a single wind turbine to assimilate more realistic observed wind profiles, with the aim of calculating more complex inflow cases that ~~retain realistic turbulent~~ don't lose their turbulent atmospheric characteristics.

An LES of a wind turbine or a wind farm, which is conducted with open lateral boundary conditions, requires, in addition to the input of the mesoscale information as horizontal mean values of the corresponding profiles, a turbulent inflow field, which synchronously feeds turbulence in the inflow region. There are different numerical approaches for generating the required turbulent inflow fields, especially for wind-turbine simulations (e.g., Bhaganagar and Debnath, 2014; Abkar et al., 2016; Englberger and Dörnbrack, 2017). One possibility is the generation of synthetic turbulence fields, as proposed by Mann (1994). These stochastic models avoid high computational costs but they are not physical models in a sense that they satisfy the conservation laws (cf. Naughton et al., 2011). Turbulent atmospheric inflow fields which are more close to observations are generated by LESs. Therefore, another possibility is the production of a limited amount of idealized precursor simulations, representing specific atmospheric conditions (neutral, convective, stable). These atmospheric precursor simulations are computationally expensive because turbulence has to spin up in the domain of interest until key flow parameters (vertical gradient of horizontal velocity, turbulence kinetic energy (TKE)) match anticipated characteristics in the ABL. Therefore, one main positive effect of the method of Nakayama and Takemi (2020) could be the application of one precursor simulation towards a variety of measurements (occurring under relatively similar atmospheric conditions, for example stratification, geostrophic winds, etc). In order to account for the broad range of possible atmospheric situations, multiple precursor simulations are required. The proposed method here is only meaningful if the measured key values of wind speed and TKE (and also lapse rate in case of stratified situations) are approximated by the precursor simulation.

The main goal of this work is the application and assessment of the vibration method in wind-energy research. Since the method can use the measured horizontal wind as a background profile, it offers a cost-effective way to simulate the effects of specific atmospheric properties on the wake of wind turbines with high spatial resolution. In general, data assimilation techniques applied in wind-energy research pose a lot of open questions (Allaerts et al., 2020, 2023; Stipa et al., 2024). With this study, we want to make a first step towards the generation of site-specific inflow fields for wind turbines using data assimilation where the additional forcing due to the assimilation is applied in a dedicated region of the computational domain upstream of the wind turbine.

The outline of this paper is as follows. The numerical model EULAG, the Newtonian relaxation methods, the vibration assimilation method, the measurements, and the numerical setup are presented in ~~Section~~ Sec. 2. In ~~Section~~ Sec. 3, we perform idealized LESs to reproduce the results of the coarse-resolution method of Nakayama and Takemi (2020). Section 4 adapts this vibration method towards a wind-energy relevant fine-resolution for their ~~NBL~~ neutral boundary layer (NBL) case. Here, we test the applicability of the vibration method at fine resolution and compare it to the performance of both Newtonian approaches. A special focus is on ~~turbulence characteristics, which would offer an answer to our first research question:~~

~~Q1 Which of the assimilation methods used is able to preserve turbulence within the scope of the defined conditions?~~

the impact of the discussed assimilation methods in regard to the characteristic atmospheric turbulence. As our final aim is to simulate real atmospheric situations, which for example may include veering inflows, ~~Section~~ Sec. 5 exemplifies how the idealized approach can be modified towards the reproduction of a measured near stable atmospheric situation in the ~~wind park~~ wind-farm WiValdi. Here, we focus on the parameter space of the vibration approach and the importance of a proper precursor simulation and use a combination of measurements and a ~~WRF~~ WRF simulation for creating ~~background~~ target wind profiles. ~~The results of this investigation allows us to answer our second research question:~~

~~Q2 Can velocities taken from precursor simulations of idealized atmospheric flows be assimilated towards arbitrary measured wind profiles?~~

Finally, we test the applicability of the vibration method in a wind-turbine simulation in ~~Section 6 , answering the third research question:~~

~~Q3 How does the wake behind a wind turbine change if velocities of idealized inflow conditions are assimilated?~~

Sec. 6 where the wind turbine is exposed to the generated inflow from Sec. 5. This is a first test case of the developed tool chain using a precursor simulation and the vibration method to generate a stably-stratified atmospheric inflow situation for a wind turbine and the subsequent simulation of the wake behind the wind turbine. Conclusions are then drawn in ~~Section~~ Sec. 7.

2 Methodology

2.1 The Numerical Model EULAG

The dry and incompressible flow inside the ABL is simulated with the geophysical flow solver EULAG (Prusa et al., 2008). EULAG is an established computational model which has been used for a wide range of physical scenarios: The simulation of urban flows (Smolarkiewicz et al., 2007), of internal gravity waves ~~(Mixa et al., 2021; ?)~~(Mixa et al., 2021; Dörnbrack, 2024), of turbulent atmospheric flows (Margolin et al., 1999), and even for the simulation of solar convection (e.g., Elliott and Smolarkiewicz, 2002). The name EULAG refers to the two possible ways to solve the equations of motion either in **EU**lerian, i.e. flux form (Smolarkiewicz and Margolin, 1993) or in semi-**LAG**rangian, i.e. advective form (Smolarkiewicz and Pudykiewicz, 1992). The advective terms in the fluid equations are approximated by the iterative finite-difference algorithm MPDATA (multidimensional positive definite advection transport algorithm) which is second-order accurate, positive definite, conservative, and computationally efficient (Smolarkiewicz and Margolin, 1998). A detailed explanation of EULAG can be found in Smolarkiewicz and Margolin (1998) and Prusa et al. (2008).

For the simulations in this study, the following set of non-hydrostatic Boussinesq equations with constant density $\rho_0 = 1.1$ kg m^{-3} are solved for the Cartesian velocity components $\boldsymbol{v} = (u, v, w)$ and for the potential temperature perturbation $\Theta' = \Theta - \Theta_e$, see Smolarkiewicz et al. (2007) in general and Englberger and Dörnbrack (2018) for wind-turbine applications:

$$\boldsymbol{\nabla} \cdot \boldsymbol{v} = 0, \tag{1}$$

$$\frac{d\boldsymbol{v}}{dt} = \underbrace{-\boldsymbol{\nabla}(\frac{p'}{\rho_0})}_{\text{pressure gradient}} + \underbrace{\boldsymbol{g}\frac{\Theta'}{\Theta_0}}_{\text{buoyancy}} \underbrace{-2\boldsymbol{\Omega} \times (\boldsymbol{v} - \boldsymbol{v}_e)}_{\text{Coriolis-Force } \mathbf{F}_{\text{cor}}} + \underbrace{\frac{\boldsymbol{F}}{\rho_0}}_{\boldsymbol{F}_{WT}} - \mathbf{f} + \mathbf{V} + \underbrace{\alpha(\boldsymbol{v} - \boldsymbol{v}_e)}_{\boldsymbol{F}_{abs}}, \tag{2}$$

$$\frac{d\Theta'}{dt} = -\boldsymbol{v}\boldsymbol{\nabla}\Theta_{\mathrm{e}} + \mathbf{H} + \beta\Theta'. \tag{3}$$

In these equations Θ_0 denotes the constant reference value of the potential temperature and Θ_e is its balanced ambient/environment state. The operators $\frac{d}{dt}$, $\boldsymbol{\nabla}$ and $\boldsymbol{\nabla}\cdot$ represent the total derivative, the gradient and the divergence. p' symbolizes the pressure perturbations, $\boldsymbol{g} = (0, 0, -g)$ is the acceleration due to gravity and $\mathbf{F}_{cor}$ indicates the Coriolis force with the angular velocity vector of the Earth ~~'s rotation Ω~~$\mathbf{\Omega} = (0, 0, \Omega sin(\phi))$, where ϕ is the latitude. The Coriolis parameter is ~~$f = 1.0 \times 10^{-4}$~~$f = 2\Omega_z = 1.0 \times 10^{-4}$ s^{-1} for midlatitudes and $\boldsymbol{v}_e$ is the background or environmental velocity.

The SGS terms $\mathbf{V}$ and $\mathbf{H}$ indicate turbulent dissipation of momentum and diffusion of heat, respectively. The simulations within this study are all conducted with a TKE closure (Margolin et al., 1999). $\mathbf{F}_{abs}$ is an absorber to ~~reduce fluctuations~~ attenuate the solution at the lateral and model top boundaries ~~.~~ (cf. Smolarkiewicz et al. (2007)). A similar absorber is used in the Eq. 3~~, where~~ . α and β ~~are~~ indicate inverse time scales. $\mathbf{f}$ denotes the additional forcing due to the selected data assimilation techniques ~~as~~ which are presented in Section 2.2, see Eqs. 4, 6, and 7.

In the simulation with a wind turbine, $\mathbf{F}_{WT}$ corresponds to the forces generated by the rotor blades. The wind turbine is implemented with the blade-element momentum theory as a rotating actuator disc (Mirocha et al., 2014). Unfortunately, the blade data for the Enercon E-115 EP3 turbine necessary for the calculation of the forces on the flow induced by the blades is currently not available. The Enercon E-115 EP3 turbines at the DLR wind park WiValdi have a hub height of $h_{hub} = 92$ m and a rotor diameter $D = 116$ m. Therefore, the simulation is conducted with the blade data of the 5 MW reference wind turbine defined by the National Renewable Energy Laboratory (NREL) (Jonkman et al., 2009). This wind turbine was selected, as it has a similar hub height ($h_{hub} = 90$ m) and rotor diameter ($D = 126$ m).

2.2 Assimilation Methods

There are several factors limiting the accuracy and comparability of LESs with real case measurements and field observations. On the one hand, the truncation errors due to discretization limit the accuracy of the numerical model (e.g., Arcucci et al., 2017; Neggers et al., 2012). On the other hand, many small-scale meteorological processes due to mesoscale phenomena, e.g. frontal passages, atmospheric waves, or diurnal circulations like land–sea breezes, can't be represented correctly by LESs (e.g., Allaerts et al., 2020). Concerning simulations with wind turbines, the grid spacing has to be small enough to account for forces generated at the blades. In a stable boundary layer (SBL), the turbulent scales are very small due to the thermal stratification and can only be partially resolved even with fine grid spacings ($dx = dy = dz \leq 5$ m). Therefore, the entire domain size of LESs is restricted to the order of kilometers and mesoscale phenomena can't be represented within these simulations, as their scales range from 10 km to more than 100 km (Haupt et al., 2022).

In order to resolve this issue, data assimilation techniques of the simulated flow field towards observational data are widely used in numerical models in order to enhance the realism of LESs. Typically the additional forcing of the assimilation is applied in the whole simulation area (e.g. Maronga et al., 2015; Allaerts et al., 2020; Stipa et al., 2024). In this work we focus on an assimilation which is only applied in a dedicated region of the simulation domain which spans the whole height (z) and width (y) of the domain but includes only a part of the streamwise length (x) of the domain. For example, the grid-nudging method relies on the definition of a local Newtonian relaxation according to Eq. 6 of Nakayama and Takemi (2020):

$$\mathbf{f}_N(x,y,z,t) = damp(x)\,\rho_0\,\frac{\boldsymbol{v}(x,y,z,t) - \boldsymbol{v}_{OBS}(z,t)}{\tau} \tag{4}$$

with

$$damp(x) = \sin^2\left[\frac{\pi}{2}\left(1 - \frac{x_{\text{nud}} - x}{x_{\text{l}}}\right)\right] \quad , \quad x_{\text{nud}} - \frac{x_l}{2} \leq \quad x \quad \leq x_{nud} + \frac{x_l}{2} \quad . \tag{5}$$

In Eq. 4, $\mathbf{f}_N$ symbolizes the forcing term $\mathbf{f}$ in the momentum conservation Eq. 2 for the local Newtonian relaxation, $\boldsymbol{v}$ is the instantaneous velocity vector at a certain grid point, and $\boldsymbol{v}_{OBS}$ is the vector of the target velocity values given through observational data. In this study, we consider only the relaxation of the zonal and meridional velocity components.

~~The Gaussian~~ As the additional forcing due to the data assimilation is only applied in a nudging area a bell-shaped damping function $damp(x)$ acts ~~only~~ in the zonal direction to prevent numerical ~~artefacts~~ artifacts at the borders of the nudging area. x_{nud} is the center of nudging area and x_{l} the length of the damping layer in the zonal direction. The relaxation time scale τ has to be chosen small enough to generate a considerable forcing towards the target data but not too small that small-scale atmospheric turbulence is suppressed (cf. Neggers et al., 2012; Maronga et al., 2015). The local Newtonian relaxation according to Eq. 4, which is introduced in Eq. 2, can provoke the damping of small-scale turbulent structures in the ABL which is mentioned by Neggers et al. (2012), Maronga et al. (2015), Heinze et al. (2017) and Nakayama and Takemi (2020).

A modification of the local Newtonian relaxation of Eq. 4 is applied by (e.g., Maronga et al., 2015; Heinze et al., 2017; Allaerts et al., 2020):

$$\mathbf{f}_{\langle N \rangle}(x,y,z,t) = damp(x)\,\rho_0\,\frac{\langle \boldsymbol{v} \rangle(z,t) - \boldsymbol{v}_{OBS}(z,t)}{\tau} \quad . \tag{6}$$

Here, a profile $\langle \boldsymbol{v} \rangle$ is computed as a spatial average over the ~~nudging zone, see~~ simulation domain. However, their approach does not include a nudging area as the additional forcing is applied in the whole domain. Instead, the present study introduces the additional forcing at every grid point in a nudging area. The formula for the calculated forcing term is identically to Eq. ~~5~~6 but the region for the averaged value includes only the nudging area with a damping function for the additional force at the borders (cf. Eq. 5). Relaxation according to Eq. 6 is referred to as Newtonian relaxation~~following Allaerts et al. (2020). There, they~~ . Allaerts et al. (2020) pointed out that this ~~approach~~ forcing term strongly overestimates the simulated TKE during daytime when applied according to their setup. A comparison of both versions of the Newtonian relaxation (applied in a nudging area) for the assimilation of an idealized NBL is presented in Section 3.

Nakayama and Takemi (2020) proposed a different way of assimilating velocities in LESs based on the vibration equation for the velocity oscillating around a zero-wind basic state with a certain frequency. They showed that their method preserves turbulent fluctuations well and can still approximate velocities to measured wind profiles. The following forcing term $\mathbf{f}_V$ is derived from the vibration equation following Eq. 7 in Nakayama and Takemi (2020):

$$\mathbf{f}_V(x,y,z,t) = damp(x)\,\rho_0\,\omega_0^2 \int\limits_0^t \Big(\boldsymbol{v}(x,y,z,t') - \boldsymbol{v}_{OBS}(z,t')\Big)dt' \quad . \tag{7}$$

Here, $\omega_0 = 2\pi f_0$ is the frequency for the oscillating velocity in the vibration equation which has to be set smaller than the peak frequency in the energy spectrum of the precursor simulation. We refer to this method in the following as the vibration method.

2.3 Measurement Data

Since November 2020, a long-range, scanning DWL has been installed at the WiValdi site to measure vertical profiles of wind speed and direction over the entire height of the ABL. The DWL is configured to measure in a velocity azimuth display (VAD) mode with a high angular resolution and a specific elevation angle to obtain accurate measurements of the mean wind vector profile as well as TKE and its dissipation rate (Wildmann et al., 2020). A microwave radiometer has also been installed along-side to obtain temperature and humidity profiles. With this combination of instruments, long-term statistics and typical characteristics of atmospheric conditions at the site can be determined (Wildmann et al., 2022).

In Section 5, the zonal and meridional velocity components of an idealized precursor simulation are assimilated towards more complex target profiles corresponding to one measured situation in a stably-stratified atmosphere. A 10 min time average profile covering the period from 1830 UTC to 1840 UTC of 19 November 2021 was selected, which features strong wind shear near the ground and a large wind veer in the ABL under weakly ~~stably stratified~~ stably-stratified conditions (confirmed by ~~analysing~~ analyzing observed vertical temperature profiles taken from the microwave radiometer). As continuous measurements are only available from $z = 57$ m up to $z = 470$ m, a simulation with WRF was performed for this period and continuous velocity profiles were generated. The WRF setup and the generation of the used target profiles is described in appendix A. We refer to the zonal and the meridional target velocities generated by the WRF simulation as target T1. As the measured velocities show a more complex structure, the WRF simulation in this work is a tool in order to generate a continuous target profile for the zonal and meridional velocities which shall reduce the uncertainty of a rough fit through the measurements. Figure 1 shows the measured velocity profiles ~~$\overline{u}_{DWL}$ and $\overline{v}_{DWL}$~~ $< u >_{DWL}$ and $< v >_{DWL}$ (uncertainties of ± 0.5 m s^{-1} are indicated by

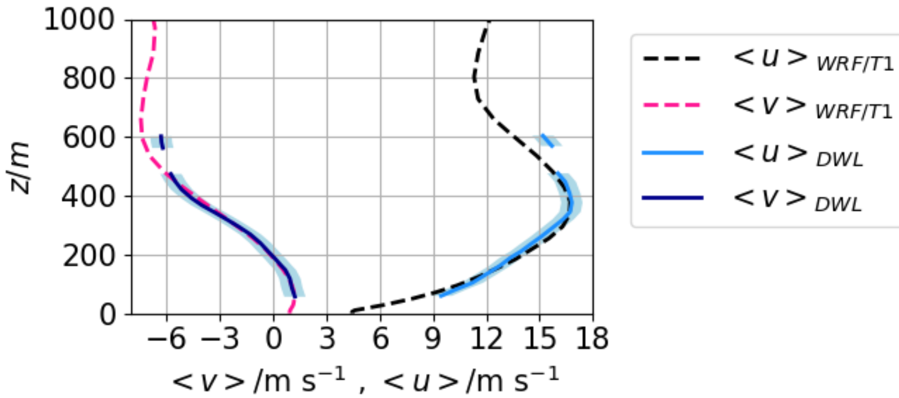

Figure 1. Vertical profiles of the measured velocities at the WiValdi site (zonal ~~$\overline{u}_{DWL}$~~$< u >_{DWL}$, meridional ~~$\overline{v}_{DWL}$~~$< v >_{DWL}$, shaded areas indicate the DWL uncertainty of ± 0.5 m s^{-1}) and the continuous profiles from the WRF simulations used as target profile T1 (zonal ~~$\overline{u}_{WRF}$~~$< u >_{WRF/T1}$, meridional ~~$\overline{v}_{WRF}$~~$< v >_{WRF/T1}$).

shaded areas (cf. Wildmann et al. (2022)) and the continuous profiles from the WRF ~~simulations $\overline{u}_{WRF}$ and $\overline{v}_{WRF}$~~simulation $< u >_{WRF/T1}$ and $< v >_{WRF/T1}$.

2.4 Numerical Setup

Table 1 gives an overview of all simulations which are performed in this study. Figure 2 shows a schematic illustration of the simulation approach used in this study. The numerical simulations are separated into precursor simulations (P1, P2 ~~,~~ and P3 in Fig. 2) and simulations with data assimilation (N1, <N1>, V1, N2, <N2>, V2 ~~,~~ and SO in Fig. 2) (+ wind turbine simulations, SW and SOW in Fig. 2). A precursor simulation is necessary so that characteristic atmospheric turbulence can spin up in the computational domain. The precursor simulations P1, P2, and P3 employ periodic lateral boundary conditions and are run until a fully developed turbulent state prevails. In the subsequent simulations, in which the output of the precursor simulations is used as the inflow field, either the local Newtonian relaxation according to Eq. 4 (N1, N2), the Newtonian relaxation according to Eq. 6 (<N1>, <N2>), or the vibration method using Eq. 7 (V1, V2, SO) are applied.

Our numerical simulations N1, <N1>, and V1 have a similar setup as those of Nakayama and Takemi (2020). N1 and V1 and are conducted to verify the correct implementation of our assimilation methods, <N1> to ~~compare with Allaerts et al. (2020)~~ investigate the effects of the Newtonian method in the presented setup with a nudging region. The sensitivity of the different assimilation methods to grid refinement is evaluated with the simulations N2, <N2>, and V2. The assimilation towards more complex target profiles for the zonal and meridional velocity components is tested in the simulation SO. As mentioned above, these profiles are close to observations at the wind farm site WiValdi (Fig. 1). While we have tested different Newtonian relaxation timescales ($\tau = 30\ s$, $\tau = 60\ s$ and $\tau = 300\ s$) and different vibration frequencies ($f_0 = 0.002$ s^{-1}, $f_0 = 0.005$ s^{-1} and $f_0 = 0.01$ s^{-1}), in this study only the results for $\tau = 30\ s$ and $f_0 = 0.002$ s^{-1} are shown. These particular values led to the closest alignment with the target profile.

Idealized cases - coarse resolution (P1, N1, <N1>, V1)

In the precursor simulation P1, a fully developed flow corresponding to an NBL with the zonal velocity profile $u = \frac{u_*}{\kappa}\ln(\frac{z}{z_0})$ (friction velocity $u_* = 0.45$ m s^{-1}, roughness length $z_0 = 0.1$ m, von Karman constant $\kappa = 0.4$) is achieved by the application of a constant pressure gradient in the horizontal direction, following Nakayama and Takemi (2020). In Fig. 2, P1 refers to this precursor simulation. The pressure gradient is implemented as an additional forcing $-u_*^2/H$ in Eq. 2 with the above mentioned friction velocity and the domain height $H = 1000$ m. For the surface friction the drag coefficient in the surface parameterization is set to 0.017, which is a requirement of EULAG's Neumann boundary conditions. The domain size is $6000 \times 6000 \times 1000$ m^3 with a grid spacing of $dx = dy = 40$ m and $dz = 10$ m. 150 000 time steps with $\Delta t = 1$ s are calculated on 100 processors in 25 hours for this precursor simulation to develop a ~~geostrophic equilibrium~~statistically stable state.

The precursor simulation is performed with periodic boundary conditions in the horizontal directions and rigid lid at the top of the domain. The Coriolis-parameter is set to zero. For the following simulation with data assimilation, synchronized 2D yz-slices are extracted at $x = 3000$ m at each time step after the simulation has reached a quasi-equilibrium state. A total of 1050 2D slices of the three velocity components and the potential temperature perturbation were taken as input at the inlet of the nudging simulation.

The nudging simulations N1, <N1> and V1 are calculated with periodic boundaries in the meridional y-direction, an open boundary condition at the zonal outflow in the x-direction, and a gradient-free, rigid-lid upper boundary. The Coriolis term in Eq. 2 is omitted in the nudging simulations, which is different to the setup of Nakayama and Takemi (2020). An explanation for this difference is given in Section 3. A nudging zone is introduced from $x = 1.0$-2.0 km over the whole lateral and vertical span of the computational domain. A logarithmic zonal target wind profile with $u_* = 0.41$ m s^{-1} and $z_0 = 0.2$ m is assumed, while the meridional target wind profile is set to 0. The three assimilation methods (Eq. 4, 6, 7) are tested separately for the adaption towards the zonal target profile in N1, <N1> and V1 respectively. Numerical absorbers (the term $\mathbf{F}_{abs}$ in Eq. 2) are included at the top above $z = 700$ m with $\alpha = 200$ s and at the outflow for $x > 5000$ m with $\alpha = 30$ s according to Smolarkiewicz et al. (2007) in order to ~~reduce numerical boundary effects.~~attenuate the solution to the prescribed states in the proximity of the open boundaries (cf. Smolarkiewicz et al. (2007)).

Idealized cases - fine resolution (P2, N2, <N2>, V2)

As wind-turbine simulations ~~require~~ especially in stably-stratified regimes are commonly computed with a higher resolution in order to resolve a large part of the turbulent structures we performed a precursor simulation P2 for the same NBL conditions as in P1 with a grid spacing of $dx = dy = dz = 5$ m. The time step has to be decreased to $\Delta t = 0.2$ s and a smaller domain of $6000 \times 3000 \times 1000$ m^3 is chosen in order to reduce the calculation time. The boundary conditions remain the same as in the coarse-grid equivalent. ~~Only the~~ The drag coefficient is ~~decreased~~ set to 0.01 ~~to fit for the velocity profile prescribed in P1.~~which leads to a vertical profile described in Sec. 2.4 after the simulation has reached a statistically stable state. Due to the smaller time step, a total of 6000 synchronized 2D yz-slices ~~are~~ is extracted from this precursor simulation for the input of the nudging simulations N2, <N2> and V2. With this high-resolved inflow the performance of the assimilation techniques

Eqs. 4, 6, 7 can be investigated. All other settings in N2, <N2> and V2, not referred to in this paragraph, are identical to N1, <N1> and V1.

~~Real~~ More realistic cases (P3, SO, SOW, SW)

In Section 5 a more complex target profile is implemented which has a zonal and a meridional component close to the measurements at the wind-farm site WiValdi (Fig. 1). Therefore, a third precursor simulation P3 is ~~conducted with~~ introduced with dominant wind shear and veer in the ABL flow. The atmospheric condition in this simulation corresponds to a stable stratification. This precursor simulation was developed by Englberger and Dörnbrack (2018) during their investigation of the impact of different thermal stratifications on wind-turbine wakes. The domain size in the simulations applying the precursor simulation P3 is 5120 × 2560 × ~~320~~430 m^3 with a grid spacing of $dx = dy = dz = 5$ m ~~.~~ in the lowest 200 m. Above 200 m the vertical spacing is dz = 10 m. For the simulation SO with nudging, the nudging zone is inserted at $x = 1.0$-2.0 km and an absorber is included for $x > 4520$ m ~~(no damping at domain top)~~with α=30 s. Due to the fact, that in an SBL negative buoyancy diminishes vertical mixing no damping layer is included at the domain top. In the corresponding wind-turbine simulation SOW the NREL 5 MW rotor is placed 200 m downstream of the nudging zone which is included from 0.5-1.5 km. The calculation time of the wind-turbine simulation is 60 min with an averaging period of the velocities of 20 min at the end of the simulation. A reference simulation SW with the wind turbine is computed with the original precursor P3 as inflow without an assimilation approach.

The assimilation methods described in Section 2.2 are only suitable if the domain averaged mean flow of the precursor simulation corresponds to the ~~domain~~ height averaged target value. This is required to preserve mass continuity (Eq. 1) in the numerical model. If there is a difference between the precursor and the target velocity profile, the horizontal mean of the vertical profile of the precursor simulation has to be normalized:

$$v_i^{new}(x,y,z) = \alpha < \overline{v}_i^p(z) >_{x,y} + v_i'^p(x,y,z) \tag{8}$$

with

$$\alpha = \frac{< v_{i,OBS} >_z}{< \overline{v}_i^P >_{x,y,z}} \quad . \tag{9}$$

Here, v_i^{new} is the new velocity value of the inflow field at every grid point, $< \overline{v}_i^p(z) >_{x,y}$ is the spacial ($<>_{x,y}$) and time-averaged mean value at every height of the precursor simulation and $v_i'^p = v_i^p - < \overline{v}_i^p(z) >_{x,y}$ is the fluctuation at every grid point i,j,k of the precursor simulation. α is derived from the division of the mean of the target profile $< v_{i,OBS} >_z$ (averaged over the height of the ABL) by the time and volume-averaged mean velocity (averaged over the last 20 min) of the precursor simulation $< \overline{v}_i^P >_{x,y,z}$.

The magnitude of the inflow field from P3 for the simulation with data assimilation SO has been modified according to Eq. 8 with $\alpha = 1.25$ ($\alpha = 0.4$) for the zonal (meridional) velocity components.

2.5 ABL and wind-turbine characteristics

In this work the following characteristics of the ABL are investigated:

Name	Precursor Simulation	Assimilation method	Grid Resolution	Target Profile
N1	P1	local Newton	coarse	idealized
<N1>	P1	Newton	coarse	idealized
V1	P1	Vibration	coarse	idealized
N2	P2	local Newton	fine	idealized
<N2>	P2	Newton	fine	idealized
V2	P2	Vibration	fine	idealized
SO	P3	Vibration	fine	WiValdi T1
SOW	P3	Vibration	fine	WiValdi T1 + wind turbine
SW	P3	-	fine	wind turbine

Table 1. Simulations conducted in this study.

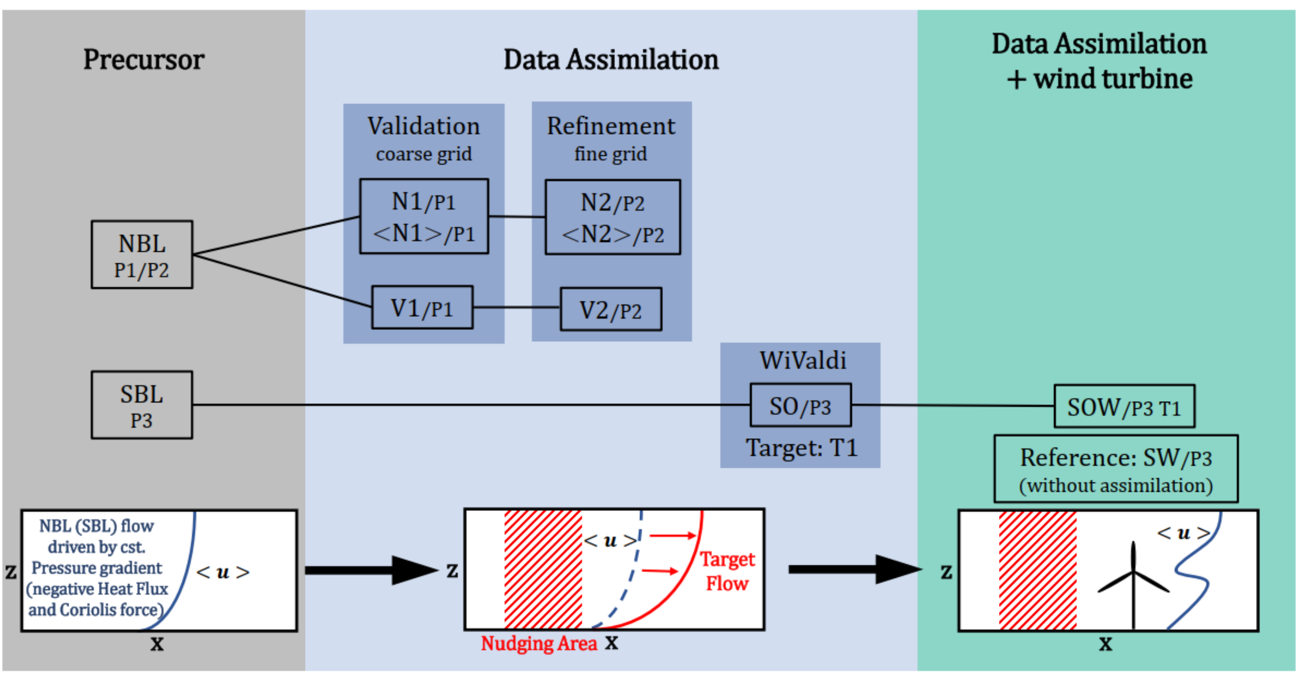

Figure 2. Schematic illustration of the different simulations considered in this study. The abbreviations indicate the simulation type following Table 1.

– The mean vertical profiles of the zonal ($< u(x_a, z) >_y$) and meridional velocities ($< v(x_a, z) >_y$) are calculated at each height level at certain downstream positions x_a averaged in the y-direction $<>_y$.

– The resolved mean TKE of the ABL

$$< TKE(x_a, z) >_y = \frac{1}{2} < (< u^{'}(x_a, y, z)^2 >_y + < v^{'}(x_a, y, z)^2 >_y + < w^{'}(x_a, y, z)^2 >_y) >_y \tag{10}$$

is calculated at each height level at certain downstream position x_a averaged in the y-direction $<>_y$. u', v' and w' are the turbulent fluctuations of the velocity components u, v and w. The fluctuations are calculated subtracting the y-averaged mean velocities from the instantaneous value at each height level. Here, $\chi^{'}(x_a, y, z) = \chi(x_a, y, z) - < \chi(x_a, z) >_y$ with χ =(u, v, w).

– The horizontal energy spectrum is calculated according to Stull (Stull, 2003, Ch. 8.6).

Concerning the wind-turbine simulations in Sect. 6 the time-averaged zonal velocity component $\overline{u_{i,j,k}}$ is shown which is averaged over the last 20 min of the simulation. The zonal velocity deficit is calculated with

$$VD_{i,j,k} \equiv \frac{\overline{u_{i_0,j,k}} - \overline{u_{i,j,k}}}{\overline{u_{i_0,j,k}}} \quad . \tag{11}$$

Here, $\overline{u_{i_0,j,k}}$ corresponds to the velocity 200 m upstream of the wind turbine in x-direction.

3 Results: Data Assimilation with coarse-grid Resolution

In this section the test scenario proposed by Nakayama and Takemi (2020) with a grid spacing of $dx = dy = 40$ m and $dz = 10$ m is reproduced in EULAG with the three different assimilation techniques described above. The aim of this section is to verify that there are no major differences in the numerical results and that EULAG is able to reproduce ~~the findings~~ similar findings like in the work of Nakayama and Takemi (2020). The results with coarse resolution are also necessary to enable a comparison with the results with a finer grid (Section 4) and they are a verification for our numerical setup without Coriolis force, which differs from Nakayama and Takemi (2020).

The results of both types of Newtonian relaxations (Eq. 4 and Eq. 6) and the assimilation method using the vibration equation (Eq. 7) are shown in Fig. 3. Vertical profiles of the zonal velocity and the resolved TKE at different downstream positions are presented. The zonal velocity component is adapted precisely towards the target profile for the two options of the Newtonian relaxation (Fig. 3 a and b). A slight overestimation of the target velocity profile by less than 0.5 m s^{-1} can be seen for the simulation with the vibration method (Fig. 3 c). In all simulations, the flow downstream of the nudging zone does not change considerably at the positions $x = 2$ km, $x = 3$ km and $x = 4$ km. The meridional velocity component is approximately zero in the precursor simulation and is not changed inside the nudging zone (not shown).

Regarding the TKE, a strong damping to values below 0.05 m^2 s^{-2} can be seen at all heights shown when the local Newtonian relaxation according to Eq. 4 is applied (Fig. 3 d). Sensitivity studies reveal that a longer relaxation time than the 30 s used here leads to smaller turbulence damping but to a poorer adjustment to the target velocity profile (not shown). This result is in agreement with previous findings by Neggers et al. (2012).

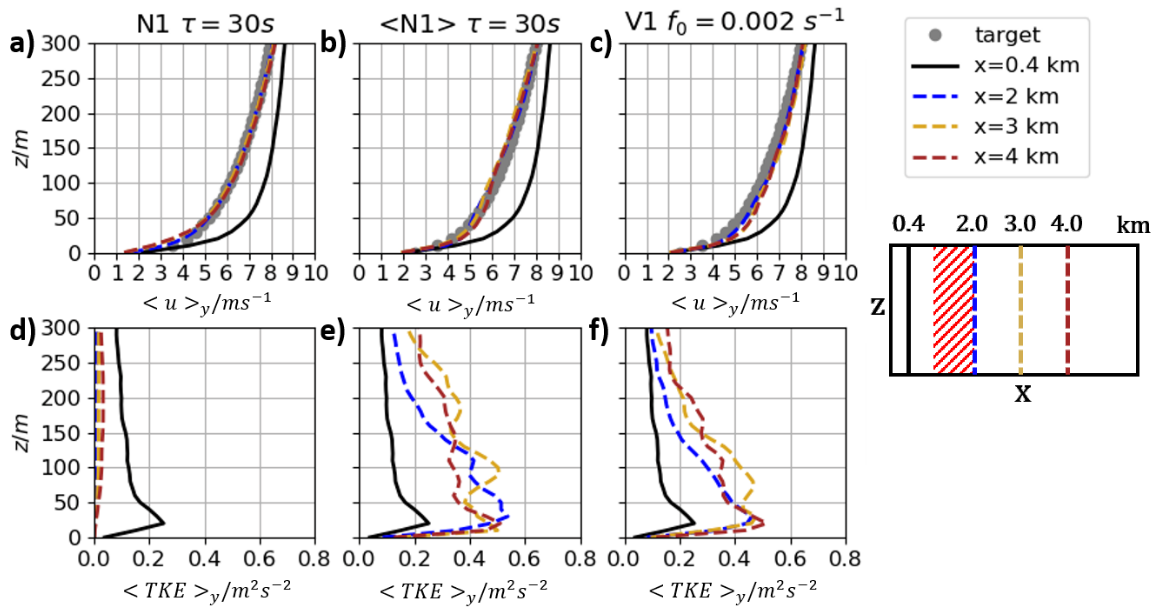

Figure 3. Results for the simulations N1, Eq. 4 and <N1>, Eq. 6 with $\tau = 30\ s$ and V1, Eq. 7 with $f_0 = 0.002$ s^{-1}. Vertical profiles of the zonal velocities $< u >_y$ in a), b) and c) and the $< TKE >_y$ in d), e) and f) for different downstream positions. The black solid lines show the quantities for the upstream flow at $x = 0.4$ km. The gray dotted lines represent the target wind profile. The blue (gold, brown) lines refer the downstream positions $x = 2$ km ($x = 3$ km, $x = 4$ km). The scheme on the right side indicates the downstream positions for the evaluation (the red hatched area refers to the nudging zone).

With the Newtonian relaxation represented by Eq. 6 instead, the TKE is 2.5 to 3 times higher when compared to the upstream values (Fig. 3 e). From this result it is concluded that TKE is not damped if the applied forcing of the assimilation method acts on the mean flow field $\langle \boldsymbol{v} \rangle$ in Eq. 6, not on the local velocity values at each grid point as in Eq. 4. The TKE is also larger than upstream of the nudging zone when the vibration method is used (Fig. 3 f) with values up to two times higher. In particular, above $z = 150$ m the increase in TKE is not as large in V1 (max. 0.18 m^2 s^{-2}) when compared to <N1> (max. 0.25 m^2 s^{-2}).

In summary, ~~our numerical results are in agreement with those of~~ similar conclusions can be drawn comparing the results in the presented study with the results from Nakayama and Takemi (2020). EULAG successfully reproduces the assimilation of the zonal velocity component towards the target profile with all three tested methods. Concerning the TKE profiles, the local Newtonian relaxation according to Eq. 4 leads to a destruction of TKE while the simulated resolved turbulence is increased for the Newtonian relaxation and the vibration method at all positions downstream of the nudging zone (when compared to the inflow TKE). ~~Our results for the Newtonian relaxation method are~~ The overestimation of the original TKE if the Newtonian method is applied is comparable to the results of Allaerts et al. (2020, 2023) ~~, while our~~ where they applied the relaxation technique in the whole domain in the precursor simulation. Our results using the vibration method are ~~in agreement with~~ similar to those of Nakayama and Takemi (2020). Both methods increase the TKE in the simulated neutral case.

~~Despite the close agreement with~~ Although similar conclusions can be drawn comparing the results in this study with the work of Nakayama and Takemi (2020), there are differences in the flow fields downstream when implementing the Coriolis force, as they do in their setup. Without Coriolis ~~forces~~force, a restoring of the ~~flow behind~~ non-assimilated upstream flow downstream of the assimilation region ~~to the initial profile~~ does not occur in our simulations, whereas it does in Nakayama and Takemi (2020). One possible reason could be their inclusion of the Coriolis force. When the Coriolis force was included in our EULAG simulations, the flow evolved temporally beyond the nudging zone away from the target profile as the Coriolis forces are applied to velocity perturbations, which are large beyond the nudging zone (Eq. 2).

4 Results: Data Assimilation within highly resolved idealized Simulations

~~For wind energy purposes~~In order to resolve smaller turbulent structures and motions, LESs with a higher resolution than that used in Sect. 3 ~~must be performed to accurately calculate the~~ are performed in this part of the study. As the power output and performance of a wind turbine is impacted directly by the atmospheric turbulence it is crucial to resolve a large part of the turbulent spectra in order to simulate the interaction of the rotor blades with the flow more precisely. Hence, the implemented assimilation methods need to be tested for higher resolved simulations with a grid-spacing of $dx = dy = dz = 5$ m (N2, <N2> and V2 in Fig. 2), i.e. with grid sizes that are ~~commonly~~ often used in wind-turbine LESs (e.g., Vollmer et al., 2016; Englberger and Dörnbrack, 2018; Chanprasert et al., 2022). In this section, we extend the work of Nakayama and Takemi (2020) and investigate the assimilation methods on a finer resolved grid.

Figure 4 a)-f) shows vertical profiles of ~~zonal velocities~~ the zonal velocity and TKE at different downstream positions for all three tested assimilation methods. This figure is directly comparable to the results of the corresponding coarse resolution simulations shown in Fig. 3. Figure 4 g)-i) present in addition the spectral energy distribution $S(k)$ as function of the wave number $k = 1/\ell(x)$, where $\ell(x)$ is the length ranging from $2\,dx$ to 500 m. The horizontal power spectra at $z = 90$ m are averaged over the y-direction and are presented for the flow upstream, inside and downstream of the nudging zone.

Starting with the local Newtonian relaxation, the zonal velocity is assimilated precisely towards the target profile for simulation N2 (Eq. 4) and does not change after the relaxation zone at $x = 3$ km or $x = 4$ km (Fig. 4 a). For this case, however, the TKE is decreased to values below 0.05 m^2 s^{-2} inside the nudging zone and further downstream. From this result, we deduce that the effect of local Newtonian relaxation on small-scale turbulence is not resolution dependent, since this is the same finding as in the corresponding coarse resolution simulation N1.

In contrast, when the Newtonian relaxation is applied in simulation <N2> (Eq. 6), the target velocity profile is underestimated by 0.8 m s^{-1} at $x = 2$ km and $z = 50$ m. At higher altitudes, the $x = 2$ km profile is consistent with the target profile (Fig. 4 b). Further downstream, at $x = 3$ km and $x = 4$ km, the velocity ~~fluctuates slightly around~~ still correlates well with the target profile ~~. This issue is probably due to the rather large~~ within a tolerance of 0.5 m s^{-1}. The TKE ~~, which~~ in this case is 2-3 times higher downstream of the nudging zone than in the upstream flow (Fig. 4 e). The ~~Newtonian relaxation~~ assimilation to the target profile in simulation <N2> (Fig. 4 b) is slightly worse than in simulation <N1> (Fig. 3 b), and the TKE is affected in the same

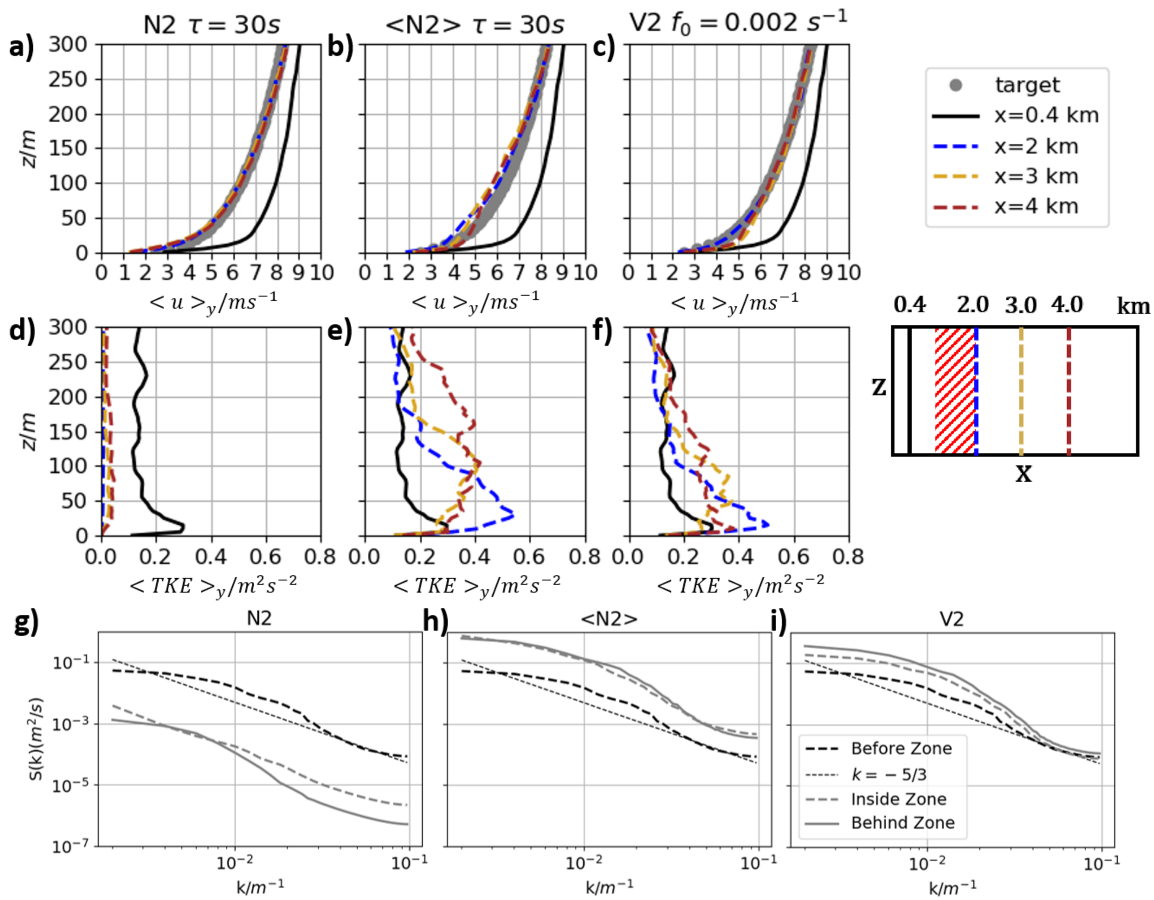

Figure 4. Results for the simulations with Newtonian relaxation N2 (Eq. 4, $\tau = 30$ s) and <N2> (Eq. 6, $\tau = 30$ s) and the vibration method V2 (Eq. 7,$f_0 = 0.002$ s^{-1}) with the fine-grid resolution. Vertical profiles of the zonal velocities $< u >_y$ in a), b) and c) and the $< TKE >_y$ in d), e), f). The black solid lines show the quantities for the upstream flow at $x = 0.4$ km. The gray dotted lines show the target wind profile. The blue (gold, brown) lines refer to the results for $x = 2$ km ($x = 3$ km, $x = 4$ km). The scheme on the right side indicates the downstream positions for the evaluation. In g), h) and i) the horizontal spectra ($z = 90$ m, length 500 m, width 3000 m) for each simulation is shown for the flow before (black dashed), inside (gray dashed) and downstream (gray solid) of the nudging zone.

way (Fig. 3 e and 4 e), which means that there is no dependence on the resolution when using the Newtonian relaxation as an assimilation method ~~for the~~ in the presented setup.

To gain a more detailed insight into the effects of the forcings applied in the simulations N2 (Eq. 4) and <N2> (Eq. 6) on the flow field, lateral cross-sections of instantaneous u and v-fields are presented in Fig. 5 a)-l). The inflow fields at $x = 500$ m are the same for the two simulations shown in Fig. 5 a) and g) and they basically represent the flow field of the precursor simulation P2. In the relaxation region, however, there is a striking difference between ~~these both Newtonian relaxation methods~~ local Newtonian and Newtonian relaxation method (Fig. 5 b and h). While in both cases the absolute value of the u-field is adjusted

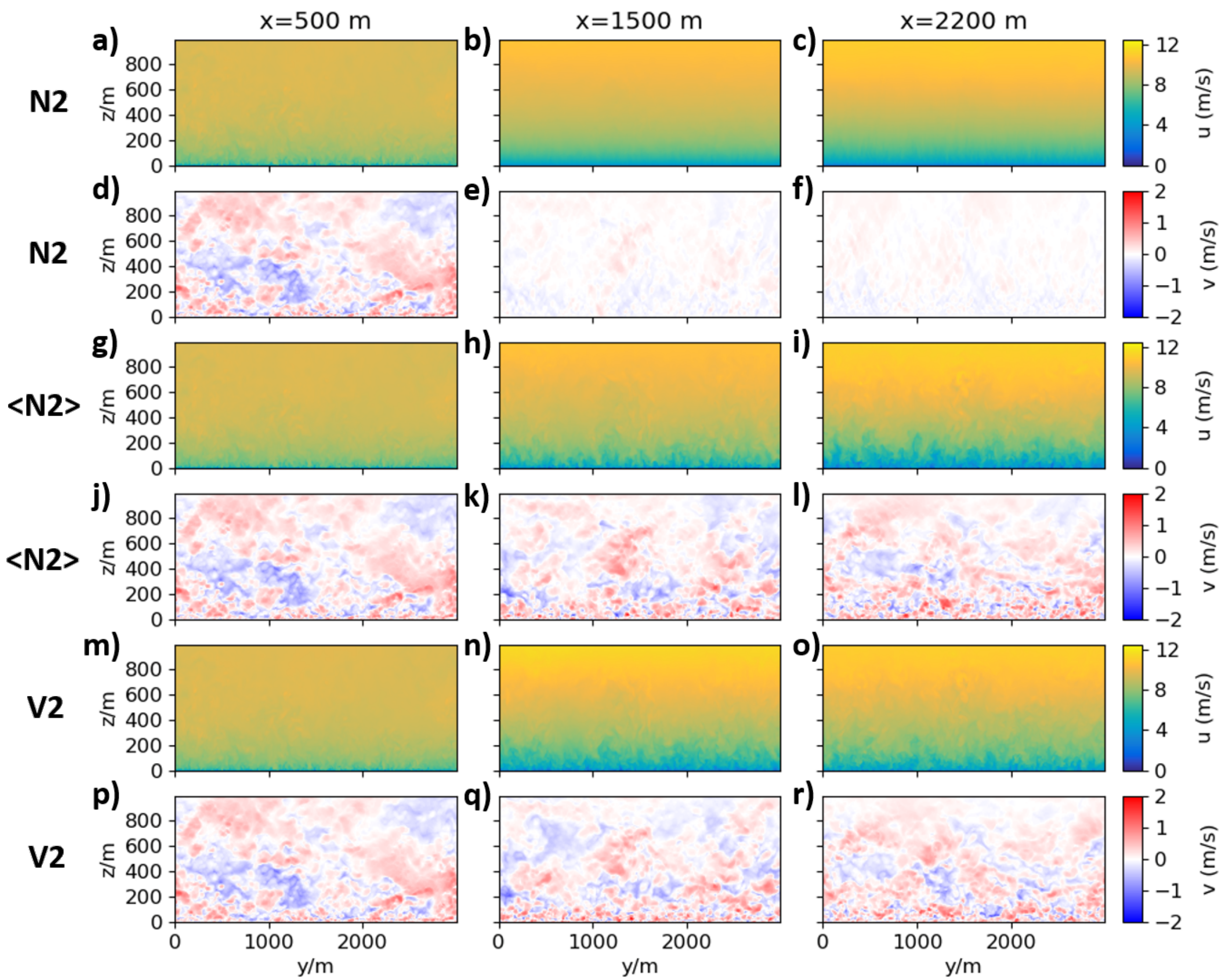

Figure 5. Vertical cross sections of the zonal and the meridional velocity u and v for $x = 500$ m upstream, $x = 1500$ m inside and $x = 2200$ m downstream of the nudging zone. The results are shown for the simulations N2 (a-f),<N2> (g-l) and V2 (m-r).

to the target profile by a deceleration of the mean flow, the flow field in simulation <N2> (Fig. 5 h) is still turbulent and no laminarization occurs, as it is the case in the simulation N2 (Fig. 5 b).

The same difference can be observed for the v-components (Fig. 5 e and k). The turbulent ~~fluctuations~~ structures of v ~~around its mean of zero are preserved~~ are not significantly altered within the relaxation region in simulation <N2> (Fig. 5 k), while they are strongly suppressed in simulation N2 (Fig. 5 e). This ~~behaviour~~ behavior in the relaxation region at $x = 1500$ m ~~, which continues downstream (~~is similar for the downstream position $x = 2200$ m~~), explains the nearly perfect adjustment of the vertical profile in simulation N2 (~~. From Fig. ~~4 a). In contrast, the small deviations of the mean u-profile that occur in~~

~~simulation <N2> are an effect of preserving the turbulence characteristics. The conclusion is that the vertical profile of the flow velocities is not meaningful on its own, but that the behavior of the is decisive~~5 it can be concluded that the turbulent structure of the eddies in the simulation domain are severely affected by the local Newtonian method, while the Newtonian relaxation and the vibration method seem to be less intrusive.

The above finding is supported by ~~analysing~~ analyzing the spectra (Fig. 4 g-h). In the case of the local Newtonian relaxation in simulation N2, the spectral energy density before the nudging (in P2) is much higher. This local Newtonian relaxation basically reduces the energy on all scales in the whole domain, resulting in a strongly reduced value of $S(k)$ to less than 10% of the inflow energy in Fig. 4 g) in comparison to Fig. 4 h) in simulation <N2>. Applying the Newtonian relaxation in simulation <N2>, the spectral energy density increases on all scales. This finding is in agreement with the increase in the resolved TKE (Fig. 4 e).

In the following, the application of the vibration method and the comparison of the corresponding simulation V2 with the simulation <N2> of the Newtonian relaxation is presented in order to investigate the difference of these two different methods on a fine grid. The vertical profile of the zonal velocity results in an exact adjustment to the target profile at $x = 2$ km (Fig. 4 c). Only at $z = 20$ m the actual velocity component is slightly overestimated compared to the target profile at $x = 3$ km and $x = 4$ km. At all other heights, the simulated velocities overlap nearly perfectly with the target profile. Figure 4 f) shows the vertical profiles of TKE. The TKE at the downstream positions is 1.5-2 times higher than in the upstream flow beneath $z = 150$ m. Above $z = 150$ m, there is only a small deviation between the downstream and upstream TKE ($\pm$ 0.06 m^2 s^{-2}).

The vibration method leads to a more precise assimilation towards the target profile in the fine-grid case of simulation V2 in comparison to the coarse-grid simulation V1 (compare Fig. 3 c and 4 c). Furthermore, the impact of the vibration method on the TKE is less pronounced for the fine-grid simulation (Fig. 4 f) than in the coarse-grid simulation (Fig. 3 f), suggesting that the vibration method performs better with higher resolution.

The impact of the different forcings **f** in Eq. 2 due to the Newtonian relaxation (Eq. 6) and due to the vibration method (Eq. 7) on the instantaneous flow field is presented in Fig. 5 g)-r) for both u and v components of simulations <N2> and V2. In general, the turbulent structure is very similar in both simulations. This could be interpreted that both assimilation methods basically impact the horizontal mean (Fig. 4 b and c) and, consequently, the resolved TKE (Fig. 4 e and f). However, the turbulent ~~3~~2 D flow structure in Fig. 5 (i, l, o, r) is only affected to a small extent. The increase of turbulence - especially below 150 m height - within and after the nudging zone compared to the region in front (Fig. 4 e-f) is partly due to an increase of $\frac{\Delta u}{\Delta z}$ in the target profile in comparison to the inflow profile of P2. It is also partly an effect of the Newtonian relaxation itself, as the v-contribution to the TKE is also larger in simulation <N2> in comparison to simulation V2, whereas $\overline{v} = 0$ in both cases (not shown).

For a more detailed comparison between the Newtonian and the vibration approach, the spectral energy density is shown in Fig. 4 h)-i) for simulations <N2> and V2. On large scales (small wave number k), the spectral power $S(k)$ increases similarly behind the nudging zone. In the nudging zone, however, the vibration method does not instantaneously reach the final spectral energy density observed behind the nudging zone. The transition occurs not as abruptly as in simulation <N2>. This abrupt transition could be an effect of the Newtonian relaxation itself applied in <N2>, which also is responsible for the higher TKE in

Fig. 4 e) in comparison to Fig. 4 f). Further, going to smaller scales (larger wave number k), the impact of the vibration method on the energy spectra decreases and for $k > 0.04$ m^{-1} an equal energy level can be seen. This is also different in comparison to the ~~behaviour~~ behavior of simulation <N2>.

All tested methods assimilate the mean flow to the target profile reasonably well. The local Newtonian relaxation method applied in N1 and N2 is not applicable for wind-turbine applications, as the TKE of the assimilated flow fields ~~becomes too small~~ is significantly reduced and the flow ~~itself too smooth~~becomes nearly laminar. It is clear that in both the vibration method and the Newtonian relaxation method, turbulence still persists after assimilation to a given target velocity profile, in comparison to the local Newtonian approach, in which a laminarization occurs. In both assimilation methods the flow is more turbulent than the inflow profile, meaning that both methods add additional turbulence. Including the spectral analysis, the integral approach of the vibration method leads to a more gentle adjustment of the energy content, while the wind profiles adjust similarly well in both approaches. The resolution impact in case of the Newtonian relaxation methods is only weakly pronounced, while the vibration method shows improved results for an increased resolution. ~~Despite these minor differences, these two methods are suitable for wind-energy applications with grid spacings of up to 5 m.~~

The coarse and fine resolution results show a very similar ~~behaviour~~ behavior of the resulting flow field ~~for~~ using the Newtonian and the vibration approach. The investigations in this section for the higher grid resolution show an improved capability of the vibration method - compared to the simulations in the coarser grid - to assimilate the mean zonal velocity component while the impact on the TKE is smaller. Compared to the Newtonian relaxation the impact on the TKE is as well less dominant when the vibration approach is applied. The following simulations, which perform an assimilation to observed profiles from the WiValdi wind park, are conducted by using the vibration method only, as, to our knowledge, this method has not been previously tested for wind-turbine relevant resolutions. ~~For a detailed investigation of the Newtonian approach for wind-energy applications and modifications of the approach itself we refer to Allaerts et al. (2020, 2023)~~ It has to be emphasized, that our approach includes a nudging region smaller than the numerical domain and omits the Coriolis-force term in the simulation with active additional forcing due to the assimilation methods. However, within the scope of interest to generate an inflow situation for a single wind turbine with small domain sizes and short simulation times, we are convinced that the presented model setup is a first step towards this final goal.

The performance of the Newtonian relaxation and possible adaptions in the model are investigated by Allaerts et al. (2020, 2023) for an assimilation which is implemented as a grid nudging method acting on every grid point in the domain while an active Coriolis-force term and pressure gradient lead to a geostrophic equilibrium in the simulation. They also investigated the vibration method, but only in combination with the Newtonian approach, with no significant difference in the ~~behaviour~~ behavior of their algorithm (Allaerts et al., 2020).

5 Results: Assimilation towards a ~~measured Wind~~ zonal and a meridional Target Profile measured in an SBL at the ~~wind-farm~~ Wind-Farm site WiValdi

The previous section has presented the efficient assimilation of the zonal velocity component in an NBL towards an idealized target wind profile for a grid spacing of $dx = dy = dz = 5$ m. In this section, ~~the continuous wind profile from the~~ a more complex stably-stratified situation is considered with an assimilation of both the zonal and the meridional wind component towards a wind profile from a WRF simulation (cf. Appendix A)~~is used as target profile for the data assimilation~~. As mentioned above in ~~Section~~Sec. 2.3, ~~this profile is close to a measured velocity profile~~ these profiles are close to measured velocity profiles from the wind-farm site WiValdi (Fig. 1) and provide continuous target profiles at each height of the domain. The objective of the simulation SO (cf. Fig. 2) is the generation of a more realistic inflow field for a wind-turbine simulation which will be discussed in Section 6. This test case in an SBL presents a preliminary step towards the application of the vibration method with the developed setup using a nudging zone in front of a wind turbine.

The data assimilation is ~~now~~ more complex, as both the zonal and the meridional components have to be adjusted to the target profiles. This extends the work of the previous chapter where the assimilation was only applied to the zonal velocity component. Hence, the simulation SO is a step towards more realistic inflow fields guided by observational data. As described above, the vibration method is used in the following for the adjustment towards the WiValdi profile.

In a first approach (not shown), we tested if the velocities of the neutral precursor simulation P2 could be assimilated towards the target profiles ~~$\overline{u}_{WRF}$ and $\overline{v}_{WRF}$~~ $< u >_{WRF/T1}$ and $< v >_{WRF/T1}$ from Fig. 1. However, the meridional velocity component in P2 is close to zero over the whole boundary layer height, while the target profile has positive values below $z = 200$ m and decreases above until -7 m s^{-1} at $z = 600$ m. This strong veer of the flow in the target profile contrasts the pure zonal flow in P2. The assimilation of the flow in P2 towards the new target profile created numerical ~~artefacts~~artifacts.

For this reason, we use another precursor simulation P3 of a stable boundary layer ~~of~~ from Englberger and Dörnbrack (2018) which has been introduced in Section 2.4. Wind shear and, in particular, wind veer both occur in this boundary layer flow. ~~The magnitude of the inflow field for the simulation with data assimilation has been modified according to Eq. 8 with $\alpha = 1.25$ ($\alpha = 0.4$) for the zonal (meridional) velocity components.~~ Figure 6 a)-b) show the mean velocities $< u >_y$ and $< v >_y$ of the modified precursor simulation for the SBL in comparison to the target velocity profiles. The results for the assimilated velocities and the TKE are shown in Fig. 6 for the ~~outflow of the nudging zone and the position 200 m~~ inflow and the positions x= 2, 3 and 4 km downstream of the nudging zone. ~~The wind turbine for the simulation presented in section 6 is located at this position.~~

With a frequency of $f_0 = 0.002$ s^{-1} in the vibration method ~~a precise~~ an assimilation towards the target zonal profile is achieved ~~above~~ beneath $z = 150$ m with a slight overestimation of <0.3 m s^{-1} (Fig. 6a). ~~Beneath~~ Above $z = 150$ m, the zonal ~~wind component~~ target is underestimated by up to 1 m s^{-1}. Figure 6 b) shows that the meridional velocity component can be adapted to the target profile with a slight underestimation (overestimation) of less than ~~0.3~~0.35 m s^{-1} between $z = 50$ m and $z =$ ~~100~~150 m ($z =$ ~~120~~240 m and $z =$ ~~250~~300 m).

Regarding the TKE, shown in Fig. 6 c), it can be seen that the turbulent regime is mostly unchanged due to the vibration method at the downstream positions. Over the whole boundary layer height the TKE stays within a range of ± 0.01 m^2 s^{-2}. The spectral analysis in Fig. 6 d) shows the spectral energy $S(k)$ at $z = 90$ m, which is close to hub height of the wind turbine in WiValdi. Similar to the neutral simulation V2, the assimilation increases the spectral energy at large scales. At small scales

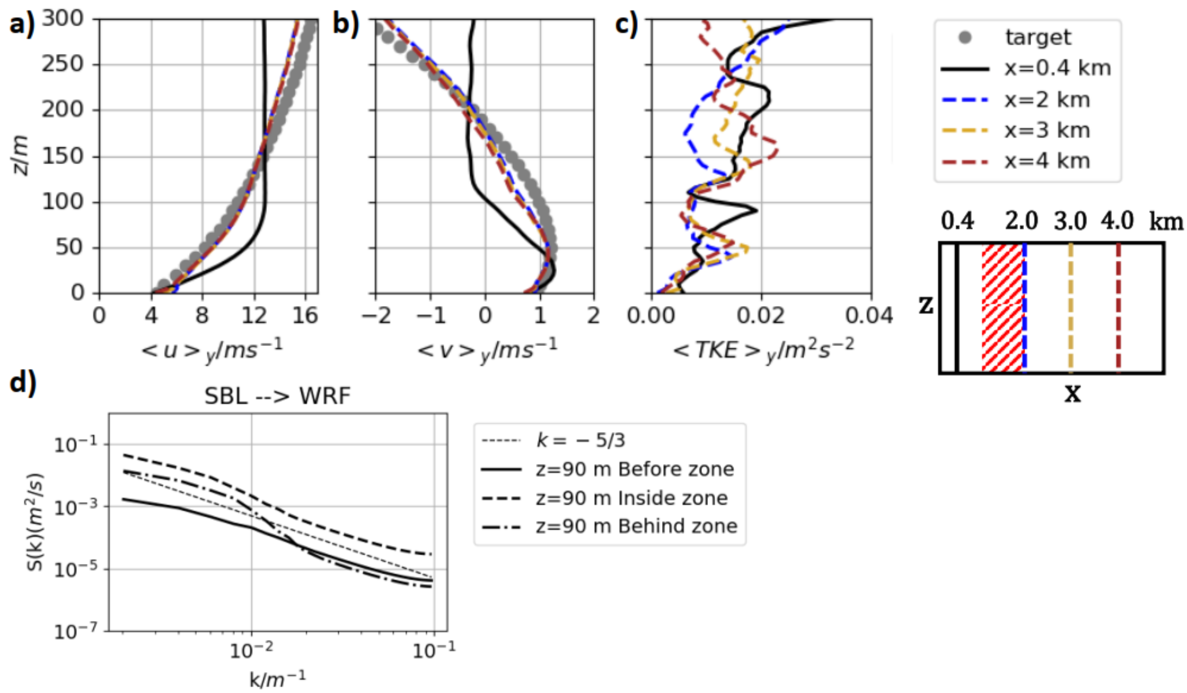

Figure 6. Results for SO of the assimilation towards the representative WRF velocity profile with the precursor simulation P3 and application of the vibration method ($f_0 = 0.002$ s^{-1}). a) zonal velocity $< u >_y$ b) meridional velocity $< v >_y$ c) $< TKE >_y$. The black solid lines refer to the values upstream of the nudging zone. The gray dotted lines in a) and b) indicate the zonal and meridional target velocity profile T2. The ~~blue~~ colored lines show the values for the ~~outflow of~~ downstream positions according to the ~~nudging zone while~~ scheme on the ~~gold lines indicate the position for the wind turbine in Sect~~right. ~~6.~~ In d) the horizontal energy spectra is shown for the height $z = 90$ m (length 500 m, width 3000 m) for the flow before, inside and behind the nudging zone.

(large k-values), ~~its comparable behind and in front~~ the spectral energy is similar upstream and downstream of the relaxation zone.

A visualization of the u and v-components of the flow for a cross-section before, inside and downstream of the nudging zone is presented in Fig. 7. In general, the upstream flow (Fig. 7 a and d) is less turbulent compared to the NBL in the previous section (e.g. Fig. 5 a and d), which is a typical characteristic of the SBL, as the only turbulence source is shear close to the surface. The adjustment of the u and v-components is clearly visible for the downstream positions while the turbulent structures are not affected considerably (Fig. 7 b, c, e, f). The zonal flow component is decelerated below 150 m in height and accelerated above. The vibration method lifts the sign-changing height of the meridional velocity component v from 100 m to 200 m. It further increases the gradient at this transition zone, while the ~~3~~2 D turbulent structure of v is not considerably changed by this process. This pattern prevails also at the wind turbine position, ~~outside~~ downstream of the nudging zone.

In summary, the wind profiles of the SBL could be adjusted efficiently towards the representative WRF velocity profiles using the vibration method. Obviously, a successful data assimilation requires that the target profiles, which prescribe

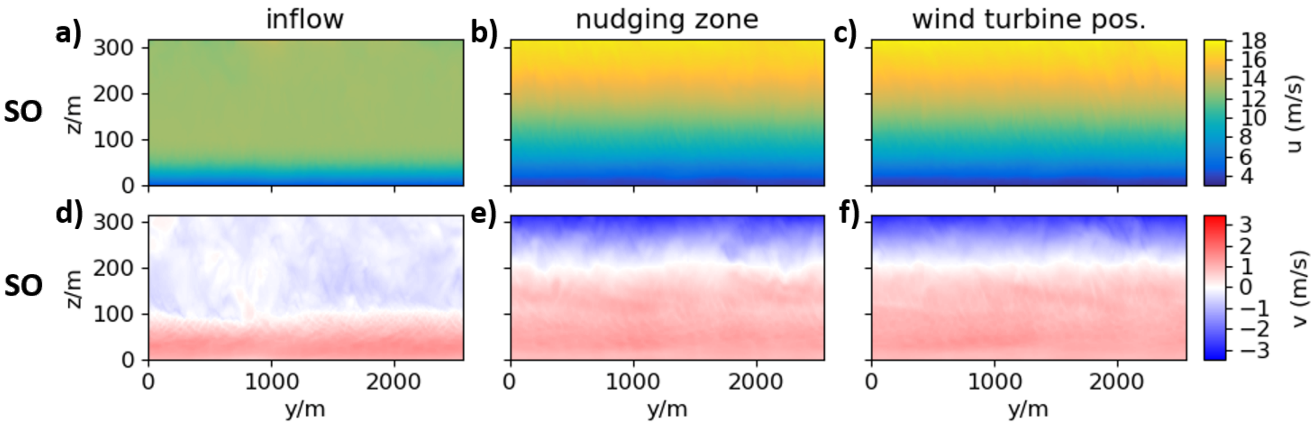

Figure 7. Vertical cross sections of the zonal and the meridional velocity u and v for the inflow area before the nudging zone (a, d), the outflow of the nudging zone (b, e) and downstream of the nudging zone at the wind turbine position (c, f). The results are shown for the simulation SO.

wind shear and veer, are ~~generated~~ approximated by a precursor simulation with similar characteristics. Furthermore, it is ~~interesting~~ remarkable that the resolved TKE in the SBL is ~~not considerably changed when using the vibration method for data assimilation, as it is in the neutral case.~~ less overestimated downstream of the nudging zone compared to the idealized neutral cases presented in Sec. 4.

~~In the previous Section 4, we have shown~~ The considered test case of the assimilation of the horizontal velocity components in an SBL shows that the velocities ~~are not changed~~ do not change considerably as the flow propagates further downstream of the nudging zone ~~. The same behavior is observed for the case discussed here. Thus, using the vibration method allows for~~ which was a unresolved issue in the setup presented by Nakayama and Takemi (2020). With the presented simulation SO which omits the Coriolis-force term and applies the vibration method in a nudging zone the inclusion of a wind turbine at a downstream position ~~,~~ after the relaxation ~~occurred~~zone seems to be reasonable. This will be presented in the next section.

6 Results: Analysis of the Wind-Turbine Wake for an assimilated Atmospheric Inflow

In this section the simulation SO presented in the previous section is repeated with the integration of a NREL 5 MW wind turbine ($h_{hub} = 90$ m, $D = 126$ m), located ~~behind~~ downstream of the nudging zone (SOW ~~) (~~in Fig. 2). The wind-turbine rotor is modeled in EULAG according to the parameterization presented in Section 2.1 and is located at $x =$ ~~2200~~1700 m, i.e. 200 m ~~behind~~ downstream of the nudging zone (from 0.5-1.5 km in SOW). Additionally, a reference simulation SW has been computed with the wind turbine exposed to the original SBL precursor simulation P3 in order to analyse the differences in the developed wakes. With this implementation ~~and comparison,~~ an efficient testing of different target wind profiles and hence different inflow fields for a wind turbine ~~can~~ could be achieved. The applicability of this approach is the objective of this section.

The time-averaged (over the last 20 min of the simulation) zonal velocity component for both cases is shown for three x - y planes covering hub height ($z = 90$ m) as well as the upper ($z = 120$ m) and lower rotor half ($z = 60$ m) of the NREL 5 MW rotor in Fig. 8. The influence of the assimilation method on the zonal velocity is clearly visible in Fig. 8 d), e) and f). The inflow velocities in front of the wind turbine are ~~reliably~~ reduced towards the target wind profile (cf. Fig. 6 a). Furthermore, the wake is deflected northwards in the assimilated simulation due to the increased vertical gradient of the meridional velocity over the upper rotor half (cf. Fig. 6 b). In contrast, the wake in the reference simulation is only deflected in the lower part of the rotor (Fig. 8 c) because wind veer only occurs in the lowest 100 m of the boundary layer in P3 (cf. Fig. 6 b, black curve). Furthermore, the deflection in the simulation SW is not as pronounced as in SOW, as the meridional wind component is smaller (v_{SW}(60 m)$<$ v_{SOW}(60 m)).

The streamwise wake extension is similar in both cases at $z = 60$ m and $z = 90$ m. A reduced wake extension is seen at $z = 120$ m for the assimilated case (Fig. 8 d). In simulation SOW, the zonal velocity deficit of 10 % is reached at $x/D = 18$ in comparison to $x/D = 22$ in the simulation without assimilation SW (Fig. 8 a). However, higher velocity deficit values are reached at similar downwind distances (20 % at $x/D = $10-12).

One reason for the reduced wake extension is the higher entrainment in the upper part of the rotor due to significantly increased vertical gradients of the zonal and meridional velocity components (Fig. 6 a and b). Another reason is the pitch angle of the blades which is 3.5° for a hub height wind speed $\overline{u} = $12-13 m s^{-1} in simulation SW while it is 0° for $\overline{u} < 12$ m s^{-1} in simulation SOW. The blades of the wind turbine in the assimilated flow field impose higher tangential and axial forces on the flow field. Further, these reasons are also responsible for the maximum velocity deficit difference in the near wake. It is 60% in simulation SOW in Fig. 8 e) and f), while it reaches only 50% in simulation ~~SO~~ SW in Fig. 8 b) and c).

Figure 9 a) and c) show the lateral view on a vertical plane through the center of the wind turbine with the visualization of the time-averaged zonal velocity component $\overline{u}$. Figure 9 b) and d) present a downstream view on the wake at $x = $5D behind the rotor. Only a part of the wake is seen in Figure 9 c) due to the deflection of the wake out of this x-z-plane. While the meridional wind component was predominant only in the lower section of the rotor in the reference case (Fig. 9 b) the assimilated wind veer (cf. Fig. 6 b) leads to a deflection of the wake over the whole rotor height in the simulation SOW (Fig. 9 d). In both cases, the wakes respond to the prevalent veer with a stretching of the wake from a circular shaped one towards an ellipsoidal shaped one, which is characteristic under veering inflow conditions.

This section presented the interaction of the wake behind the rotor within a stable atmospheric boundary-layer flow. The results for both simulations ~~are in good accordance to other studies from Bhaganagar and Debnath (2014), Abkar and Porté-Agel (2015) and Englberger and Dörnbrack (2018)~~ show the main features of a wind-turbine wake in an SBL. The asymmetry and elliptic shape of the wake (cf. Fig.9) are as well described by Abkar and Porté-Agel (2015) (Fig.17) and Englberger and Dörnbrack (2018) (Fig.6) who considered wind-turbine wakes in SBLs ~~. The~~ too. The deflection of the wake if wind veer is dominant in near-stably stratified ABL regimes is also described by Bhaganagar and Debnath (2014) (Fig.11) and Mirocha et al. (2015) (Fig.11). The applied vibration method adapts the wind profile to the target profile and changes wind veer and shear in the atmospheric flow accordingly. Due to these changes of the mean inflow conditions, the developed wake is different in its shape and also considering the velocity deficit compared to the reference case ~~without assimilation. Currently, there~~ SW. There is

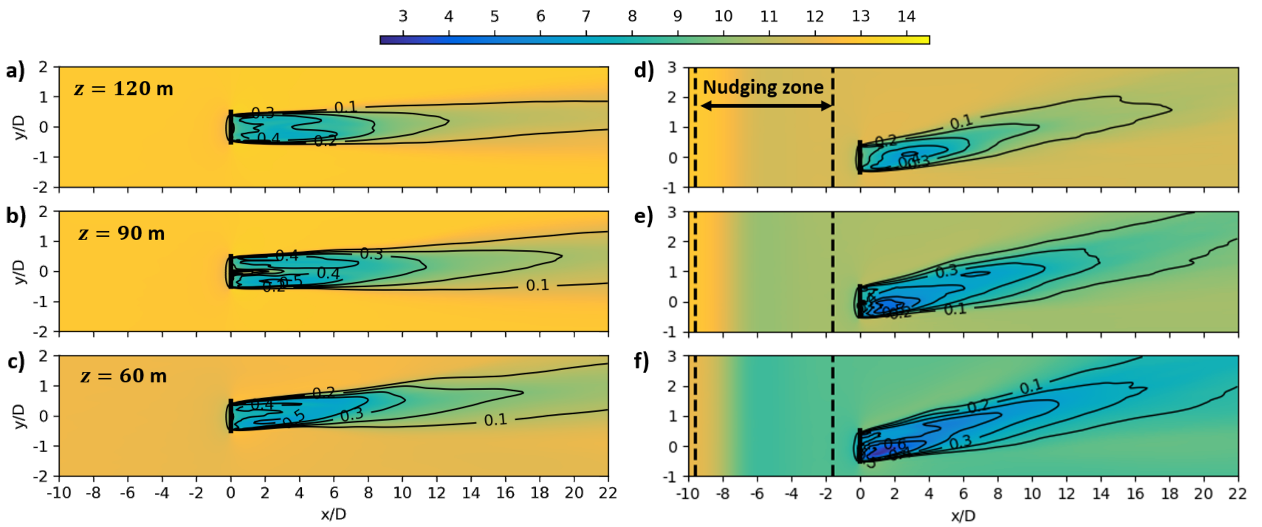

Figure 8. Coloured contours of the time-averaged zonal velocity component $\overline{u_{i,j,k}}$ in m s^{-1} ~~without data assimilation~~ for SW in a), b) and c) and ~~with vibration assimilation~~ for SOW in d), e) and f) averaged over 20 min at the end of the simulation. b) and e) show the x - y plane at hub height $z = 90$ m. a) and d) (c and f) correspond to the x - y planes at $Z = 90m + R/2 = 120$ m ($Z = 90m - R/2 = 60$ m). The black contours represent the velocity deficit $VD_{i,j,k}$ at the same vertical location calculated in relation to the upstream velocity at $x = $-200 m. The axes are normalized by the rotor diameter D = 126 m, whereby $x/D = 0$ indicates the position of the rotor.

no measurement data available for wakes behind the wind turbines at the wind-farm site WiValdi for the considered situation. Therefore, a ~~more quantitative analysis~~ validation of the wake against observations could not be done at this point. However, the results of this section present the first step towards an efficient method to generate inflow fields for a single wind turbine in a near-stably stratified ABL.

7 Conclusions

~~A systematic sensitivity study with s investigating the impact~~ The applicability of two versions of Newtonian relaxation and a vibration method within a dedicated nudging area in an LES has been investigated in this study. A systematic sensitivity study on a coarse (spatial resolution of 40 m) and a fine (spatial resolution of 5 m) numerical grid has been performed for an NBL. The coarse resolution results are ~~compatible with the previous study of Nakayama and Takemi (2020).~~ similar to the findings in the study from Nakayama and Takemi (2020). However, the presented setup in this study omits the Coriolis-force term in the simulations with data assimilation in order to avoid the evolution of the mean profiles downstream of the nudging area. With the fine resolution simulations, the differences of the two Newtonian relaxation methods and the vibration method could be investigated in detail, showing a very similar performance in adjusting the horizontal mean wind to the target velocity profile. In the case of the Newtonian and the vibration approach, the TKE as well as the power spectra are influenced by

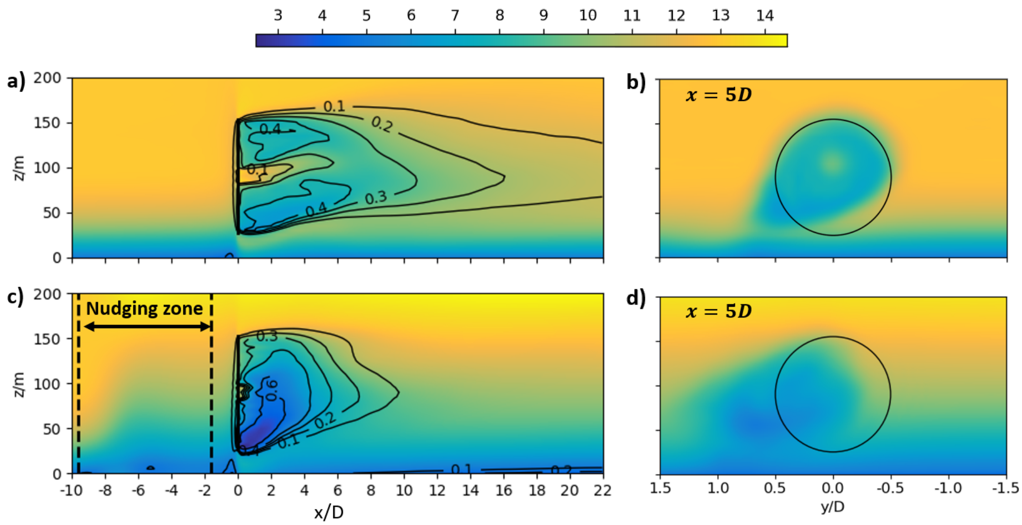

Figure 9. Coloured contours of the time-averaged zonal velocity component $\overline{u_{i,j_0,k}}$ in m s^{-1} without assimilation in a) and b) and with vibration assimilation in c) and d) averaged over 20 min at the end of the simulation. In a) and c) the vertical x - z plane at the position $y = 0$ perpendicular to the turbine is presented. The black contours represent the velocity deficit $VD_{i,j_0,k}$ at the same spanwise location calculated in relation to the upstream velocity at x = -200 m. The abscissa is divided by the diameter of the rotor, whereby $x/D = 0$ indicates the position of the rotor. b) and d) show zonal velocity component at a downward position of x = 5D. The black circles represent the rotor area.

the relaxation, ~~whereas the 3 D~~ but turbulent structures are ~~preserved~~not damped like in the case of the local Newtonian approach. The impact of the vibration method in the spectra sets in more slowly in comparison to a more abrupt transition with Newtonian relaxation. This results in a TKE difference compared to the inflow, which is less pronounced when using the vibration method. Therefore, the data assimilation technique using the vibration equation achieved the most reliable results and could be successfully validated on a fine grid, necessary ~~in wind-energy applications~~if smaller turbulent structures have to be resolved.

The vibration method has been applied with a frequency of $f_0 = 0.002$ s^{-1} to adjust velocities from an idealized precursor simulation towards a ~~measured~~ representative wind profile for the wind farm site WiValdi. In particular, at heights below 60 m, the target profile obtained by measurement data is supplemented by data extracted from a mesoscale model simulation. The ~~resulting profiles were used as inflow for the 5MW NREL wind turbine to test the applicability of the vibration method in combination with a rotor. The developed wake under two inflow conditions, the pure precursor inflow and the assimilated inflow, was compared and analysed regarding the temporal averaged zonal wind and the velocity deficit, resulting in a consistent wake pattern. The differences arise mainly from the different horizontal velocity values of the vertical profiles in the precursor simulation in comparison to the measured profile. The~~ present study provides a first insight of the ~~vibration method~~ assimilation of mean velocities using the vibration method and the consecutive response on turbulence characteristics in LESs for the generation of site-specific inflow fields for wind turbines.

The comparative analysis of the implemented vibration method with both Newtonian methods has shown the different impact on turbulence statistics. ~~Based on the results achieved, the first research question can be answered: Which of the assimilation methods used is able to preserve turbulence within the scope of the defined conditions?~~ We conclude that all assimilation approaches modify the simulated turbulence. The local Newtonian relaxation leads to a laminarization of the flow. In contrast, Newtonian relaxation and the vibration methods amplify the turbulent perturbations. Although none of the methods tested perfectly preserves the turbulence of the inflow, the methods that do not lead to complete decay are therefore preferable. ~~There is the potential to improve the method further to more closely assimilate to the inflow turbulence. For the Newtonian method , Allaerts et al. (2020, 2023) did a first step into this direction. A similar approach is necessary for the vibration method in future.~~Of course this aim is only reasonable, if the precursor simulation is set up in order to approximate the turbulent characteristics of on-site measurements as close as possible. Another important aspect is potential temperature, especially when it comes to stably-stratified atmospheric regimes. Although the influence of the vibration method in combination with a nudging zone on the potential temperature (not shown) does not impact the horizontal velocity components in the presented SBL, an implementation of a potential temperature nudging would be favorable when it comes to the stratification of potential temperature in the considered atmospheric situation (cf. Allaerts et al. (2020)).

In this work, two different highly resolved precursor simulations are applied. We found that the vibration method is only applicable when the basic atmospheric conditions and the target profile are relatively close to each other in structure, e.g. either veering inflow or pure zonal flow. It was not possible to assimilate a precursor simulation with no meridional wind component to a veering target profile. ~~These results of the numerical simulations answer our second research question, namely whether velocities taken from precursor simulations of idealized atmospheric flows can be assimilated towards arbitrary measured wind profiles. In these arbitrary profiles there must be a~~ Under this precondition, the presented setup with a nudging zone in the numerical domain has proven its utility to assimilate the mean inflow velocities towards a desired target velocity profile which propagates further downstream. Hence, computational time can be saved for the generation of atmospheric inflow fields for a wind turbine, if the main characteristics of the precursor simulation (vertical gradient of horizontal velocity, TKE) and the atmospheric measurements are similar.

Although these first results are very promising, the presented simulations omit the Coriolis force. It should be noted that our non-hydrostatic numerical model has only the pressure perturbation as a diagnostic variable, which is determined by integrating an elliptic equation and whose solutions are used as corrections to make the wind field divergence-free, as required by the continuity equation. This means, from the Navier-Stokes equations the hydrostatic equation $\frac{\partial p}{\partial z} = -\rho g$ is subtracted to obtain the governing equations solved by EULAG. Therefore, only pressure perturbations appear in the pressure gradient term. In a similar way, horizontal pressure gradients proportional to a geostrophic wind (here: u_e and v_e) can be subtracted leading to the ~~meridional wind . Since only one precursor simulation has to be performed to adapt the simulated velocities to different expected target profiles of flows, the presented numerical setup has the ultimate advantage of saving computational resources for long and expensive simulations.~~Coriolis-terms $\sim (u - u_e)$ and $\sim (v - v_e)$. It is important to note that EULAG always solves for deviations from these (hydrostatic or geostrophic) balanced states (Smolarkiewicz and Margolin, 1997). By omitting the Coriolis force, our numerical simulations are limited to small domains on the order of kilometers and short simulation periods (<1 h in this study). As a consequence, the developed setup would be a useful tool for the generation of atmospheric inflow fields for single wind turbines - as well as two wind turbines like in the case of WiValdi - but forbids its application for large wind farms, where the balance between pressure gradient and Coriolis force is crucial for a realistic representation of the atmospheric flow (cf. Bastankhah et al. (2024)). The generation of atmospheric flows which are in a geostrophic balance by means of a grid nudging method with application of the additional forcing in the whole domain is presented by Allaerts et al. (2020).

Finally, the assimilated flow field was used as inflow for a wind turbine simulation which was parameterized with the blade element momentum method as rotating actuator disc~~, providing an answer to the third research question of how the wake behind a wind turbines changes if velocities of idealized precursor simulations are assimilated~~. The differences in the wake behind the wind turbine (wake deflection, wake elongation, velocity deficit) performed with the assimilated flow field in comparison to the one with the inflow of the non-assimilated pure precursor simulation, can be traced back to the differences in the horizontal mean of the inflow velocities (e.g. increase of vertical gradient of zonal and meridional flow). The wake structures (ellipsoidal in lateral cross section, wake deflection due to wind direction changing with height) are in agreement with many previous publications (e.g. Abkar et al., 2016; Vollmer et al., 2016; Bhaganagar and Debnath, 2014; Englberger and Dörnbrack, 2018). The assimilation itself did not influence these structures as it was to be expected from the fact that the vibration method only adapts the mean value of the wind speed, while attaining the turbulent ~~3 D~~ structures. This result makes the vibration method suitable and attractive for wind-turbine simulations. The DWL-measurements that were used in this study were taken at a time when wind turbines were still under construction at the WiValdi ~~windpark~~wind park, so that measurement data for wind turbine wakes is not available for this time in order to provide a comparative analysis with observations. A logical next step would be to extend the current work by assimilating to a profile at a time in which nacelle-based lidar wake measurements are available also (since November, 2023). However, this work presents the utility of the developed approach with a grid nudging region upstream of the wind turbine leading to an assimilated velocity inflow profile for a wind turbine.

~~Our setup offers two advantages when compare to the setup of Allaerts et al. (2020) and Allaerts et al. (2023): Our setup has the possibility to assimilate simultaneous (time varying) measurements, as it works with open horizontal boundary conditions. Further, it is basically applicable in complex terrain. Its value in these areas has to be tested in future studies, but the general requirements are fulfilled.~~

Appendix A: WRF Setup

The wind profiles used as target velocity profiles in Sect. 5 and Sect. 6 were extracted from a simulation performed with the WRF model version 4.4.1. A particular time period during 19.11.2021 was chosen from DWL-observations taken at the research wind farm located at Krummendeich (cf. Sect. 2.3). On this day the DWL-observations showed that the conditions at the wind park represented a quasi-neutral boundary layer with nominal wind speeds at hub height of roughly 10 m s^{-1}.

The WRF simulation consists of four nested domains, with a horizontal grid spacing of 5 km, 1 km, 200 m and 40 m for domains 1-4, respectively. The domains with sub-kilometer grid spacing are run in LES mode. Vertical nesting is applied also, so that higher vertical resolution is used in the domains with higher horizontal resolution. The mean target profiles for the zonal and meridional velocity used in EULAG are extracted from D4 and vertically interpolated so that there is a constant $dz = 5$ m. Initial and boundary conditions are supplied from the European Centre for Medium-Range Weather Forecasts (ECMWF) operational analyses, which has a temporal resolution of 6 h. Topography data for the LES domains are provided by the Copernicus digital elevation model and are available at a horizontal grid spacing of 90 m and 30 m. The model top was set at about 12 km height to include tropopause effects. A 3 km upper damping layer is implemented, to restrict reflection of gravity waves. The Monin-Obukhov scheme is used to simulate the surface layer (Janjic (1996)). Additionally, the Noah-MP land-surface model (Niu et al. (2011)), the Rapid Radiative Transfer Model long-wave scheme (Mlawer et al. (1997)), the Dudhia short-wave scheme (Dudhia (1989)), the WRF single-moment five-class microphysics scheme (Hong and Lim (2006)) are used. In domains 1 and 2 the Kain–Fritsch cumulus parameterization scheme is implemented (Kain and Fritsch (1990)) and a planetary boundary scheme is used, namely the Mellor–Yamada–Janjic TKE scheme (Mellor and Yamada (1982)). In the LES domains (domains 3-4) the cumulus parameterization and planetary boundary schemes are switched off, and SGS turbulence is parameterized by a three-dimensional 1.5-order TKE closure (Deardorff (1980)). The simulations were performed for a total of 7 hours, from 12 UTC to 19 UTC on 19.11.2021.

Author contributions. All authors conceived the idea and contributed to the manuscript. LW performed the simulations and visualisation. LW and AE did the conceptual design. NW performed the DWL and MWR measurements and GK computed the WRF simulation.

Competing interests. The contact author has declared that neither of the authors has any competing interests.

Acknowledgements. Measurements at the WiValdi research park (https://windenergy-researchfarm.com/) were conducted as part of the research project Deutsche Forschungsplattform für Windenergie (http://dfwind.de). We greatly acknowledge the financial support of the German Federal Ministry for Economic Affairs and Climate Action, through FKZ 0325936, that enabled this work. The authors gratefully acknowledge the Gauss Centre for Supercomputing e.V. (http://www.gauss-center. eu) for funding this project by providing computing time on the GCS Supercomputer SuperMUC at Leibniz Supercomputing Centre (LRZ, www.lrz.de). Funding was provided by German Aerospace Center (DLR e.V.).

References

Abkar, M. and Porté-Agel, F.: Influence of atmospheric stability on wind-turbine wakes: A large-eddy simulation study, Physics of fluids, 27, 035 104, https://doi.org/https://doi.org/10.1063/1.4913695, 2015.

Abkar, M., Sharifi, A., and Porté-Agel, F.: Wake flow in a wind farm during a diurnal cycle, Journal of Turbulence, 17, 420–441, 2016.

Aitken, M. L., Kosović, B., Mirocha, J. D., and Lundquist, J. K.: Large eddy simulation of wind turbine wake dynamics in the stable boundary layer using the Weather Research and Forecasting Model, Journal of Renewable and Sustainable Energy, 6, 2014.

Allaerts, D., Quon, E., Draxl, C., and Churchfield, M.: Development of a time–height profile assimilation technique for large-eddy simulation, Boundary-Layer Meteorology, 176, 329–348, 2020.

Allaerts, D., Quon, E., and Churchfield, M.: Using observational mean-flow data to drive large-eddy simulations of a diurnal cycle at the SWiFT site, Wind Energy, 26, 469–492, 2023.

Arcucci, R., D'Amore, L., Pistoia, J., Toumi, R., and Murli, A.: On the variational data assimilation problem solving and sensitivity analysis, Journal of Computational Physics, 335, 311–326, 2017.

Bastankhah, M., Mohammadi, M. M., Lees, C., Diaz, G. P. N., Buxton, O. R., and Ivanell, S.: A fast-running physics-based wake model for a semi-infinite wind farm, Journal of Fluid Mechanics, 985, A43, 2024.

Bhaganagar, K. and Debnath, M.: Implications of Stably Stratified Atmospheric Boundary Layer Turbulence on the Near-Wake Structure of Wind Turbines, Energies, 7, 5740–5763, https://doi.org/10.3390/en7095740, 2014.

Chanprasert, W., Sharma, R., Cater, J., and Norris, S.: Large Eddy Simulation of wind turbine wake interaction in directionally sheared inflows, Renewable Energy, 201, 1096–1110, 2022.

Deardorff, J. W.: Stratocumulus-capped mixed layers derived from a three-dimensional model, Boundary-layer meteorology, 18, 495–527, 1980.

Dörnbrack, A.: Transient Tropopause Waves, Journal of the Atmospheric Sciences, 81, 1647–1668, 2024.

Dudhia, J.: Numerical study of convection observed during the winter monsoon experiment using a mesoscale two-dimensional model, Journal of Atmospheric Sciences, 46, 3077–3107, 1989.

Elliott, J. R. and Smolarkiewicz, P. K.: Eddy resolving simulations of turbulent solar convection, International Journal for Numerical Methods in Fluids, 39, 855–864, 2002.

Englberger, A. and Dörnbrack, A.: Impact of neutral boundary-layer turbulence on wind-turbine wakes: a numerical modelling study, Boundary-Layer Meteorology, 162, 427–449, https://doi.org/https://doi.org/10.1007/s10546-016-0208-z, 2017.

Englberger, A. and Dörnbrack, A.: Impact of the Diurnal Cycle of the Atmospheric Boundary Layer on Wind-Turbine Wakes: A Numerical Modelling Study, Boundary Layer Meteorology, https://doi.org/https://doi.org/10.1007/s10546-017-0309-3, 2018.

Hansen, M.: Aerodynamics of Wind Turbines, Earthscan, https://books.google.de/books?id=GVD_HDPix6YC, 2013.

Haupt, S. E., Kosovic, B., Berg, L. K., Kaul, C. M., Churchfield, M., Mirocha, J., Allaerts, D., Brummet, T., Davis, S., DeCastro, A., et al.: Lessons learned in coupling atmospheric models across scales for onshore and offshore wind energy, Wind Energy Science Discussions, 2022, 1–36, 2022.

Heinze, R., Moseley, C., Böske, L. N., Muppa, S. K., Maurer, V., Raasch, S., and Stevens, B.: Evaluation of large-eddy simulations forced with mesoscale model output for a multi-week period during a measurement campaign, Atmospheric Chemistry and Physics, 17, 7083–7109, 2017.

Hong, S.-Y. and Lim, J.-O. J.: The WRF single-moment 6-class microphysics scheme (WSM6), Asia-Pacific Journal of Atmospheric Sciences, 42, 129–151, 2006.

Janjic, Z.: The Mellor-Yamada level-2.5 scheme in the NCEP Eta model, in: Preprint, 11ˆ< th> AMS Conference on Numerical Weather Prediction, Norfolk, VA, 1996, 1996.

Jonkman, J., Butterfield, S., Musial, W., and Scott, G.: Definition of a 5-MW Reference Wind Turbine for Offshore System Development, https://doi.org/10.2172/947422, 2009.

Kain, J. S. and Fritsch, J. M.: A one-dimensional entraining/detraining plume model and its application in convective parameterization, Journal of Atmospheric Sciences, 47, 2784–2802, 1990.

Kilroy, G., Englberger, A., Wrba, L., Bührend, L., and Wildmann, N.: Evaluation of turbulence characteristics in WRF simulations at WiValdi wind park, Journal of Physics: Conference Series, 2767, 052 063, https://doi.org/10.1088/1742-6596/2767/5/052063, 2024.

Mann, J.: The spatial structure of neutral atmospheric surface-layer turbulence, Journal of fluid mechanics, 273, 141–168, https://doi.org/https://doi.org/10.1017/S0022112094001886, 1994.

Margolin, L. G., Smolarkiewicz, P. K., and Sorbjan, Z.: Large-eddy simulations of convective boundary layers using nonoscillatory differencing, Physica D: Nonlinear Phenomena, 133, 390–397, 1999.

Maronga, B., Gryschka, M., Heinze, R., Hoffmann, F., Kanani-Sühring, F., Keck, M., Ketelsen, K., Letzel, M. O., Sühring, M., and Raasch, S.: The Parallelized Large-Eddy Simulation Model (PALM) version 4.0 for atmospheric and oceanic flows: model formulation, recent developments, and future perspectives, Geoscientific Model Development, 8, 2515–2551, 2015.

Mellor, G. L. and Yamada, T.: Development of a turbulence closure model for geophysical fluid problems, Reviews of Geophysics, 20, 851–875, 1982.

Mirocha, J., Kosovic, B., Aitken, M., and Lundquist, J.: Implementation of a generalized actuator disk wind turbine model into the weather research and forecasting model for large-eddy simulation applications, Journal of Renewable and Sustainable Energy, 6, 013 104, https://doi.org/https://doi.org/10.1063/1.4861061, 2014.

Mirocha, J. D., Rajewski, D. A., Marjanovic, N., Lundquist, J. K., Kosović, B., Draxl, C., and Churchfield, M. J.: Investigating wind turbine impacts on near-wake flow using profiling lidar data and large-eddy simulations with an actuator disk model, Journal of Renewable and Sustainable Energy, 7, 2015.

Mixa, T., Dörnbrack, A., and Rapp, M.: Nonlinear Simulations of Gravity Wave Tunneling and Breaking over Auckland Island, Journal of the Atmospheric Sciences, 78, 1567 – 1582, https://doi.org/10.1175/JAS-D-20-0230.1, 2021.

Mlawer, E. J., Taubman, S. J., Brown, P. D., Iacono, M. J., and Clough, S. A.: Radiative transfer for inhomogeneous atmospheres: RRTM, a validated correlated-k model for the longwave, Journal of Geophysical Research: Atmospheres, 102, 16 663–16 682, 1997.

Nakayama, H. and Takemi, T.: Development of a Data Assimilation Method Using Vibration Equation for Large-Eddy Simulations of Turbulent Boundary Layer Flows, Journal of Advances in Modeling Earth Systems, 12, e2019MS001 872, 2020.

Naughton, J., Balas, M., Gopalan, H., Gundling, C., Heinz, S., Kelly, R., Lindberg, W., Rai, R., Saini, M., and Sitaraman, J.: Turbulence and the isolated wind turbine, in: 6th AIAA theoretical fluid mechanics conference, p. 3612, 2011.

Neggers, R. A., Siebesma, A., and Heus, T.: Continuous single-column model evaluation at a permanent meteorological supersite, Bulletin of the American Meteorological Society, 93, 1389–1400, 2012.

Niu, G.-Y., Yang, Z.-L., Mitchell, K. E., Chen, F., Ek, M. B., Barlage, M., Kumar, A., Manning, K., Niyogi, D., Rosero, E., et al.: The community Noah land surface model with multiparameterization options (Noah-MP): 1. Model description and evaluation with local-scale measurements, Journal of Geophysical Research: Atmospheres, 116, 2011.

Porté-Agel, F., Bastankhah, M., and Shamsoddin, S.: Wind-turbine and wind-farm flows: A review, Boundary-layer meteorology, 174, 1–59, 2020.

Prusa, J. M., Smolarkiewicz, P. K., and Wyszogrodzki, A. A.: EULAG, a computational model for multiscale flows, Computers and Fluids, 37, 1193–1207, https://doi.org/https://doi.org/10.1016/j.compfluid.2007.12.001, 2008.

Rybchuk, A., Martínez-Tossas, L. A., Letizia, S., Hamilton, N., Scholbrock, A., Maric, E., Houck, D. R., Herges, T. G., de Velder, N. B., and Doubrawa, P.: Ensemble-Based, Large-Eddy Reconstruction of Wind Turbine Inflow in a Near-Stationary Atmospheric Boundary Layer Through Generative Artificial Intelligence, Wind Energy, 28, e70 020, 2025.

Sanchez Gomez, M. and Lundquist, J. K.: The effect of wind direction shear on turbine performance in a wind farm in central Iowa, Wind Energy Science, 5, 125–139, 2020.

Skamarock, W. C., Klemp, J. B., Dudhia, J., Gill, D. O., Liu, Z., Berner, J., Wang, W., Powers, J., Duda, M., Barker, D., et al.: A description of the advanced research WRF version 4, NCAR tech. note ncar/tn-556+ str, 145, 2019.

Smolarkiewicz, P. K. and Margolin, L. G.: On Forward-in-Time Differencing for Fluids: an Eulerian/Semi-Lagrangian Non-Hydrostatic Model for Stratified Flows, Atmosphere-Ocean, 35, 127–152, https://doi.org/10.1080/07055900.1997.9687345, 1997.

Smolarkiewicz, P. K. and Margolin, L. G.: MPDATA: A Finite-Difference Solver for Geophysical Flows, Journal of Computational Physics, 140, 459–480, https://doi.org/https://doi.org/10.1006/jcph.1998.5901, 1998.

Smolarkiewicz, P. K. and Margolin, L. O.: On forward-in-time differencing for fluids: Extension to a curvilinear framework, Monthly Weather Review, 121, 1847–1859, 1993.

Smolarkiewicz, P. K. and Pudykiewicz, J. A.: A class of semi-Lagrangian approximations for fluids, Journal of Atmospheric Sciences, 49, 2082–2096, 1992.

Smolarkiewicz, P. K., Sharman, R., Weil, J., Perry, S. G., Heist, D., and Bowker, G.: Building resolving large-eddy simulations and comparison with wind tunnel experiments, Journal of Computational Physics, 227, 633–653, https://doi.org/https://doi.org/10.1016/j.jcp.2007.08.005, 2007.

Spille-Kohoff, A. and Kaltenbach, H.-J.: Generation of turbulent inflow data with a prescribed shear-stress profile, in: DNS/LES Progress and challenges, pp. pp–319, 2001.

Stauffer, D. R. and Seaman, N. L.: Use of four-dimensional data assimilation in a limited-area mesoscale model. Part I: Experiments with synoptic-scale data, Monthly Weather Review, 118, 1250–1277, 1990.

Stipa, S., Ajay, A., Allaerts, D., and Brinkerhoff, J.: TOSCA–an open-source, finite-volume, large-eddy simulation (LES) environment for wind farm flows, Wind Energy Science, 9, 297–320, 2024.

Stull, R. B.: An introduction to boundary layer meteorology, 2003.

Veers, P., Bottasso, C. L., Manuel, L., Naughton, J., Pao, L., Paquette, J., Robertson, A., Robinson, M., Ananthan, S., Barlas, T., et al.: Grand challenges in the design, manufacture, and operation of future wind turbine systems, Wind Energy Science, 8, 1071–1131, 2023.

Vollmer, L., Steinfeld, G., Heinemann, D., and Kühn, M.: Estimating the wake deflection downstream of a wind turbine in different atmospheric stabilities: an LES study, Wind Energy Science, 1, 129–141, https://doi.org/10.5194/wes-1-129-2016, 2016.

Wharton, S. and Lundquist, J. K.: Atmospheric stability affects wind turbine power collection, Environmental Research Letters, 7, 014 005, https://doi.org/10.1088/1748-9326/7/1/014005, 2012.

Wildmann, N., Päschke, E., Roiger, A., and Mallaun, C.: Towards improved turbulence estimation with Doppler wind lidar velocity-azimuth display (VAD) scans, Atmospheric Measurement Techniques, 13, 4141–4158, https://doi.org/10.5194/amt-13-4141-2020, 2020.

Wildmann, N., Hagen, M., and Gerz, T.: Enhanced resource assessment and atmospheric monitoring of the research wind farm WiValdi, in: Journal of Physics: Conference Series, vol. 2265, p. 022029, IOP Publishing, 2022.